

Seasonal to decadal variability in ice discharge from the Greenland Ice Sheet.

Michalea D. King, Ian M. Howat, Seongsu Jeong, Myoung J. Noh, Bert Wouters, Brice Noël, and Michiel R. van den Broeke

Author Response

We thank the referees for their careful review, thorough comments, and constructive tone. We have used their valuable feedback to improve the description of methodological details, broaden discussion, add two new figures, and enhance the bibliography with key references. These changes and have allowed us to improve the original manuscript.

We have responded to point-by-point comments from Reviewer 1, followed by Reviewer 2, below. Referee comments are listed in *italics*, immediately followed by our response. The revised manuscript is included as a separate document.

Reviewer 1

Overall, this is a really good paper. It's well written and focused with a clear message. It is a useful and interesting study, which adds to the literature. My comments are fairly minor and are in the attached pdf.

Response: We thank the reviewer for their comments and helpful suggestions.

1. Abstract

Would be helpful to give date range in abstract. Also gives context for how many seasonal cycles these seasonal values are based on.

Response: We amended the phrase “derive ice discharge...for the 21st century” to instead read “derive ice discharge...for the 2000-2016 period” on page 1, line 16.

Please indicate somewhere in the abstract how many glaciers you include and whether they cover the entire ice sheet. Also, how were they selected? Perhaps you include all glaciers larger than a certain size, but would be helpful to indicate how comprehensive the sample is here.

Response: We inserted the following text to line 15 of the abstract: “Here we sample outlet glaciers wider than 1 km (N =230) to derive the first...”

2. Introduction

Page 1, Line 30

SWIPA 2017

Page 2, line 3

Add citation *Andersen, M.L., L. Stenseng, H. Skourup, W. Colgan, S.A. Khan, S.S. Kristensen, S.B. Andersen, J.E. Box, A.P. Ahlstrøm, X. Fettweis and R. Forsberg, 2015. Basin-scale partitioning of Greenland ice sheet mass balance components (2007–2011). Earth and Planetary Science Letters, 409:89-95.*

Page 2, Line 6

Carr, J. R., A. Vieli, and C. R. Stokes 2013. Climatic, oceanic and topographic controls on marine-terminating outlet glacier behavior in north-west Greenland at seasonal to interannual timescales, Journal of Geophysical Research, 118(3), 1210-1226.

Page 2, line 11

<https://www.the-cryosphere-discuss.net/tc-2018-17/>

Page 2, Line 12

Howat et al., 2008

Response: We inserted the five references listed above into the manuscript. Note that the authors could not locate the exact article with the title provided for the Carr et al. 2013 reference. We instead referenced the article below, which is the final publicized title of the article the reviewer suggested:

Carr, J. R., Vieli, A. and Stokes, C.: Influence of sea ice decline, atmospheric warming, and glacier width on marine-terminating outlet glacier behavior in northwest Greenland at seasonal to interannual timescales, *J. Geophys. Res. Earth Surf.*, 118(3), 1210–1226, doi:10.1002/jgrf.20088, 2013.

Page 12, Line 13

You articulate the issue clearly

Response: The authors appreciate the positive feedback on writing style and clarity.

Page 2, Line 14

It'd be useful to define 'shorter' and 'longer' term. These can mean very different things to different people.

Response: We replaced the phrase “longer record” with “decadal records”, and “shorter term” with “seasonal to sub-monthly.”

Page 2, Line 15

Again, indicating temporal resolution here would support his statement, e.g. do you have data every month? Every day?

Response: We changed “Here we present the first continuous record of net ice sheet discharge, derived over the 2000–2016 period” to instead read “Here we present the first continuous record of daily estimates of net ice sheet discharge, derived over the 2000–2016 period”.

3. Data and Methods

Page 2, Line 20

As noted in the abstract, it would be helpful to indicate which glaciers you use, how many, and how they were selected for context.

Response: We replaced “derive discharge...for *each* glacier” with “230 glaciers with widths greater than 1 km”.

Page 2, Line 27

Please indicate the bed / ice thickness errors, e.g. mean error and range for your study glaciers.

Response: We added the text ‘Bed topographic errors across our sampled flux gates average 70 ± 52 m’.

Page 3, Line 5

Sounds odd. Rephrase. E.g. ...estimates from velocity data that were mostly collected between....

Response: We amended the phrase to read “Enderlin et al. (2014) derived annual discharge estimates from velocity data that were mostly collected between April and September.”

Page 3, Line 14

Do you have a threshold for the number of monthly observations? It could cause problems if you have only one year of data if it happens to be a particularly fast or slow year. Please indicate how you have accounted for this.

Response: The standard seasonal curve is derived by using median values for months where at least 5 years of data for that month exist. We have clarified this on Page 2, Line 19 of the Supplementary material.

Page 3, Line 15

How reasonable is it to do this? I'd like to see this supported by e.g. applying this function to each month where you do have data and checking how close a fit the periodic function is. I would also imagine the goodness of fit of this function would vary by glacier / area, so this should also be assessed. Finally, please make it clear how many glaciers / records this effects: if it is an occasional thing for a few glaciers, it probably has minimal impact on results, but if it's several months for each glacier, that could have a big impact. At the moment, it's unclear which is the case.

Response: All glaciers have periods of missing velocity data at some point throughout the time series. Most of the missing periods are in the early record when only velocities derived from optical data, and thus months of solar insolation, are available. The number of months requiring modeled data vary by year and by glacier. To clarify our use of a periodic function, we added the following text to Page 3, Line 15:

“The periodicity described here does not indicate that a symmetric, sinusoidal seasonality is assumed, but rather that by detrending the time series and isolating a mean seasonal pattern of change, we would expect the endpoints of the curve to be the same (i.e. the 12-month curve would repeat).

Page 3, Line 20

What is your threshold for the data being 'too sparse' and therefore not included?

Response: We have added the following text to clarify:

“This data sparsity occurs when months of missing data exceed the number of months containing reliable observations post-filtering, preventing a resolvable seasonality.”

Page 4, Line 24

Would be useful to have a map showing which glaciers you did / didn't include.

Response: We added a figure to the Supplementary material (now Figure S4) that satisfies this suggestion as well as the second figure suggestion listed below.

4. Results

Page 5, Line 3

Perhaps you do this later in the paper, but it would be interesting to look at the sources of these changes. E.g. do ~70% come from a few glaciers, and we should therefore focus on those? You could perhaps make a 'hotspot map' to show which locations are hotspots of variability / ic loss and colour code according to time. I'm suggesting this because it would be a useful guide for where people should focus their attention and highlight how this has changed over time. E.g. are KG and HH still really important or has this shifted?

OK, you do this later in the paper. However, please consider whether you can show the shifting of these 'hotspots' of individual glaciers graphically, to really emphasise the (important) point. E.g. a map with symbols sized according to discharge contribution and coloured by date.

Response: We have added a figure (Figure S4) to the Supplementary Material that shows the location of all sampled glaciers, as well as highlights the average and cumulative discharge anomaly of the 20 largest glaciers over 2 periods (2000-2008 and 2008-2016).

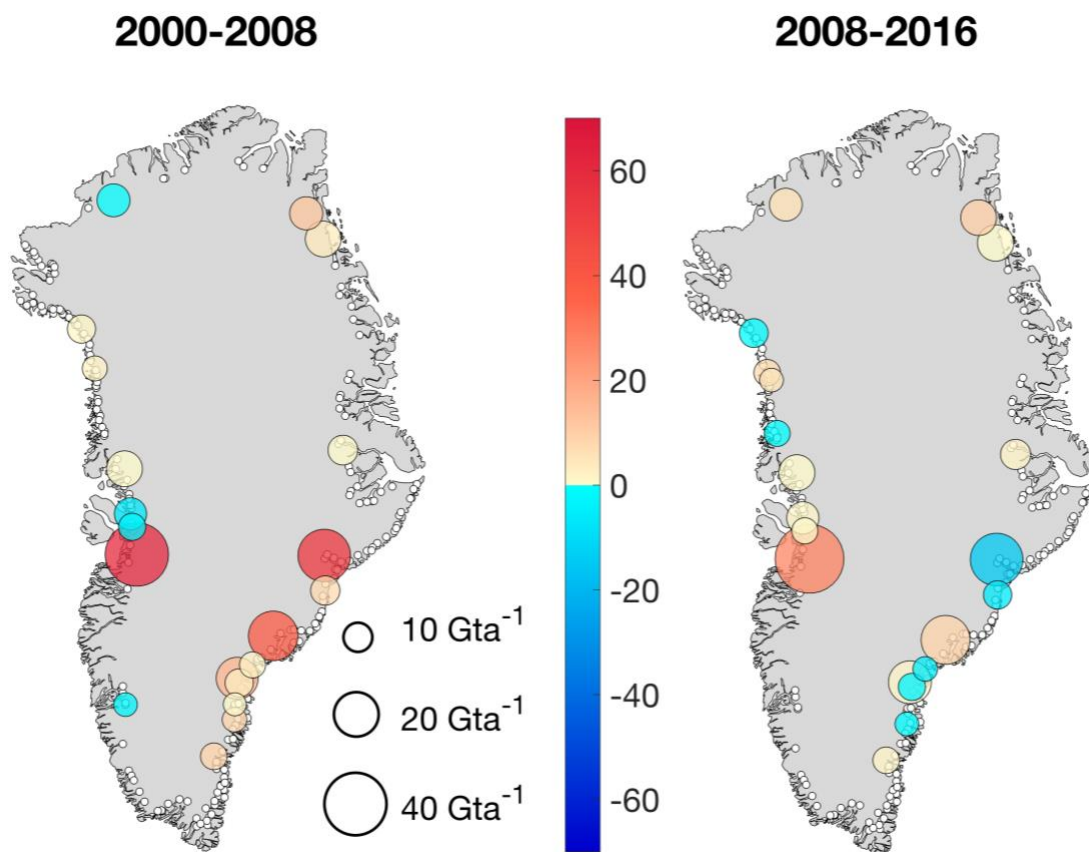


Figure S4: Spatial distribution of all surveyed glaciers, denoted by a white marker near the flux gate of each glacier. The 20 largest glaciers are shown by colored markers, with the marker size corresponding to the average D over both the 2000–2008 period (left) and 2008–2016 period (right). The color of the markers shows the total D anomaly (in Gta^{-1}) relative to the reference years 2000 (left) and 2008 (right). Positive discharge anomalies indicate increased D relative to the reference years.

Page 5, Line 18

low? I.e. the seasonal decline was less than in other years?

Response: We replaced “shallow” with “reduced relative to other years”.

Page 6, Line 18

It would be interesting to see how the seasonal amplitude differs between terminus type, i.e. floating versus grounded tongues. I guess you may pick this up in your regional values, because they are all in the north.

Response: The proposed scientific question is an interesting one, and we agree that glacier geometry is relevant to observed seasonal amplitude at the individual glacier scale. We consider the further subdivision of regional glacier groupings by geometric parameters, such as terminus type, outside the scope of the current manuscript, but may be the subject of future work.

Page 6, Line 21

This suggest there may be issues with using the sinusoidal cycle to fill the data gaps.

Response: The standard seasonal curve at each glacier, including Jakobshavn, represents a median cycle of seasonal change over all years, including both those with a more even, sinusoidal variability and years with non-symmetric patterns of change. While this method assumes the glacier's "typical" pattern of change to predict values during missing periods, it is also informed by nearby available observations. We note that velocity observations (typically available through September in the early part of the time series) show no clear indication of a secondary period of acceleration, and we expect that the seasonality earlier in the study period would most closely resemble years nearest in time (i.e. 2009-2011, which are fully resolved via available InSAR data). Please see our response to the above comment on Page 3, Line 15, which includes added text to clarify this point. We also added the text "...and represents a "typical" pattern of change at each respective glacier" to Page 3, Line 13 for clarity.

Page 7, Line 16

Please check the official name of this glacier. My understanding is it is called either Nioghalvfjerdingsfjorden Glacier or 79 North Glacier.

Response: We replaced all references to this glacier with "79 North Glacier".

Page 7, Line 28

Previous work has noted an increase in variability in retreat rates in SE Greenland from 2010 onwards (link below). Perhaps this is just a coincidence, but could a reduced seasonal amplitude be linked to more variable retreat rates? E.g. if lower seasonality means some glaciers stay on each a bed rock ridge? Just something to think about.

<https://www.cambridge.org/core/journals/journal-of-glaciology/article/ice-front-change-of-marinerterminating-outlet-glaciers-in-northwest-and-southeast-greenland-during-the-21st-century/B737AD36ECBDB86F51FADD65A686B3BB>

Response: This is an excellent point and worth consideration. We have enhanced the discussion (Page 11, Line 16) by adding the following text:

"Recent work by Bunce et al. 2018 describes increased interannual variability in SE front position, due to asynchronous retreat observed at glaciers in that region. This asynchrony may also contribute to the more recent muted seasonality in the SE region, as previously described."

Page 8, Line 5

I'd say that we can expect seasonal or shorter variations in D associated with runoff. A number of studies (e.g. Tedstone et al., 2015, nature); Sundal et al 2012; Schoof 2010) have demonstrated that meltwater inputs have limited impact on interannual ice velocities. I think it is still valuable to test it, but this progress in the temperature should be acknowledged.

Response: We agree that adding more context to the current body of work on temporal limitations of meltwater impacts will enhance the discussion. We added the following text and three references to the discussion on Page 11, Line 21:

“Previous work focused on land-terminating glaciated regions of the GrIS (Sundal et al 2011; Tedstone et al. 2015) and work using modeled channelization processes (Schoof 2010) demonstrated that meltwater impacts on glacier velocities operate on narrow temporal windows and may even result in a net deceleration on seasonal to annual timescales.”

1. Schoof, C.: Ice-sheet acceleration driven by melt supply variability, *Nature*, 468(7325), 803–806, doi:10.1038/nature09618, 2010.
2. Sundal, A. V., Shepherd, A., Nienow, P., Hanna, E., Palmer, S. and Huybrechts, P.: Melt-induced speed-up of Greenland ice sheet offset by efficient subglacial drainage, *Nature*, 469(7331), 521–524, doi:10.1038/nature09740, 2011.
3. Tedstone, A. J., Nienow, P. W., Gourmelen, N., Dehecq, A., Goldberg, D. and Hanna, E.: Decadal slowdown of a land-terminating sector of the Greenland Ice Sheet despite warming, *Nature*, 526(7575), 692–695, doi:10.1038/nature15722, 2015.

Page 8, Line 23

Typo

Response: Corrected.

Page 8, Line 23

Where are these regional correlations shown? It'd be helpful to have a set of figures like the one for the whole population, but for each region or a table. This is an important point, so could be added to the main paper. This way, all of the correlations can be seen and compared.

Response: We agree with the reviewer that these figures should be included in the main body to improve the paper. We have added the regional correlations to Figure 5 as suggested.

Page 8, Line 24

Reference the relative figure.

Response: Reference to Figure 5 added.

Page 8, Line 26

Why should this correlate? Briefly explain the logic here. Delayed response to terminus retreat? We'd expect the near-front ice velocities to respond immediately, so are you suggesting this is due to longer-term draw down?

Response: Some of this relationship may be due to the annual grouping of front positions and discharge. For example, front position can continue to retreat at some glaciers into the fall, after the typical summer peak in discharge. If autumn/wintertime discharge rates remain elevated as a result of continued retreat through December of the previous year, the following spring/summertime acceleration would be superimposed on a higher base discharge rate.

For clarity, we added the following text to Page 8, Line 26:

“We test for these lagged relationships between retreat and annual D to account for the temporal grouping of the data. For example, front position may continue to retreat into the autumn, after the typical peak in D . If autumn/wintertime discharge rates remain elevated as a result of continued retreat through December of the previous year, we would anticipate the following springtime acceleration to be superimposed on a higher base discharge rate.”

Page 9, Line 9

Why this value?

Response: Due to the long-tailed distribution of seasonal runoff data, daily runoff with values greater than the 50% percentile make up the majority (~95%) of the total seasonal runoff. To clarify, we added the following text to Line 9: “We use this threshold as a way to delineate the onset of significant runoff by separating days with negligible runoff contributions from those with non-negligible runoff contributions.”

Page 9, Line 12

Yes, but it still only explains 33% of the variance, so there's 77% it doesn't explain.

Response: We amended the phrase “Significant correlations...indicating that a later onset in runoff tends to correlate with a later peak in *D*” to instead read “indicating that a later-occurring peak *D* may be related to later onset of runoff” to more appropriately frame the significant relationship as only one component of the observed variability.

Page 10, Line 7

See also Andersen et al 2015 (reference above).

Response: We added the text “Annual *D* estimates for 2007 and 2011 are approximately 5 % and 7 % lower than those estimated in Andersen et al. 2015, but also within margins of uncertainty” to Page 10, Line 9.

Page 10, Line 9

So gives higher velocity values and therefore higher discharge

Response: Text added.

Page 10, Line 16

Reference the paper / figure showing the GRACE data you are discussing here.

Response: Reference to Figure S5 (now S6) added.

Page 10, Line 28

As noted above, Bunce et al 2018 saw an increase in FP variability in the SE at this time, so it might be worth noting this and considering if there is any link between the two.

Response: Please see our added text to Page 11, Line 16, as described in a previous response above.

Page 11, Line 6

Reference relevant figure.

Response: Reference to Figure S9b (now S10b) added.

Page 11, Line 16

Add a couple of key additional references - this has been said elsewhere..

Response: We have added the following citations:

Nick, F. M., Vieli, A., Howat, I. M. and Joughin, I.: Large-scale changes in Greenland outlet glacier dynamics triggered at the terminus, Nat. Geosci., 2(2), 110–114, doi:10.1038/ngeo394, 2009.

Vieli, A. and Nick, F. M.: Understanding and Modelling Rapid Dynamic Changes of Tidewater Outlet Glaciers: Issues and Implications, *Surv. Geophys.*, 32(4–5), 437–458, doi:10.1007/s10712-011-9132-4, 2011.

5. Conclusions

Page 12, Line 7

Is this change effected in any way by increasing data availability after e.g. Landsat 8 came online?

Response: We reason that changes in data availability do not significantly impact the long-term changes described here, although increased data does reduce errors and improve the resolution of seasonal variability. The increased discharge observed since 2000 is also present when using data from only the summertime periods, when temporal data availability is common for all years. We also use RADARSAT data for validation as described in the supplementary material.

Page 13, Line 8

*Carr, J.R., Stokes, C.R. and Vieli, A., 2017. Threefold increase in marine-terminating outlet glacier retreat rates across the Atlantic Arctic: 1992–2010. *Annals of Glaciology*, 58(74), pp.72-91.*

Page 13, Line 9

*Bartholomaus, T.C., Stearns, L.A., Sutherland, D.A., Shroyer, E.L., Nash, J.D., Walker, R.T., Catania, G., Felikson, D., Carroll, D., Fried, M.J. and Noël, B.P., 2016. Contrasts in the response of adjacent fjords and glaciers to ice-sheet surface melt in West Greenland. *Annals of Glaciology*, 57(73), pp.25-38.*

*Catania, G.A., Stearns, L.A., Sutherland, D.A., Fried, M.J., Bartholomaus, T.C., Morlighem, M., Shroyer, E. and Nash, J., 2018. Geometric Controls on Tidewater Glacier Retreat in Central Western Greenland. *Journal of Geophysical Research: Earth Surface*, 123(8), pp.2024-2038.*

*Carr, J. R., A. Vieli, C. R. Stokes, S. S. R. Jamieson, S. Palmer, P. Christoffersen, J. A. Dowdeswell, D. Blankenship, and D. Young (2015), Basal topographic controls on rapid retreat of Humboldt Glacier, northern Greenland, *Journal of Glaciology*, 61, 137-150.*

*Porter, D.F., Tinto, K.J., Boghosian, A., Cochran, J.R., Bell, R.E., Manizade, S.S. and Sonntag, J.G., 2014. Bathymetric control of tidewater glacier mass loss in northwest Greenland. *Earth and Planetary Science Letters*, 401, pp.40-46.*

Response: We added the citations above.

6. Figures

Page 27, Figure 5

It would be useful / interesting to do this for each region.

Response: We updated Figure 5 to also show regional correlations discussed for the NW and SE regions.

Reviewer 2

Review of King, Howat et al. This is an excellent, clearly written and carefully considered observational paper on the relationship of ice flow and discharge with a number of variables from climate or ice geometry for the Greenland Ice Sheet. I can be accepted as it is.

While strong in its observational detail, it raises a heap of questions about how the system works in detail, now that we ‘see’ the real details. Untangling these will give rise to a number of papers in the future, and I suspect many of them will cite this paper as a basis for general statements about what the observational data (and observation driven modelling, RACMO) have to say about the ice sheet.

Response: We thank the reviewer for their comments and helpful suggestions.

Page 7, Line 23-34

This would seem to be the crux of the paper. The identification of a ‘ubiquitous’ seasonal variability, for all Greenland glaciers on average, around 6% when normalized per glacier, begs for some kind of explanation. Moreover, the fixed timing of the seasonal peak is curious since several causes of the seasonal increase are identified – loosening of sea ice / mélange in the fjords, seasonal component of ice front retreat, meltwater drainage and lubrication, ocean-driven basal melting (to the extent that it is seasonal), and possibly some sort of R-channel closure late in the season (e.g. Jacobshavn second peak). In the last sentence of this section, the uniformity of the timing of the peak argues that the dominant cause of variation is summer melting somehow - -yet runoff peaks are different from D peaks. You discuss this in 3.4, but seem to point to a process or mechanism (maybe more than one) that sits between a direct correlation of D and runoff, since the size of runoff seems to have less impact on the size of seasonal max in D and timing can vary (is this because runoff timing in heavy snow areas like the SE is not the same as peak melting?)

Response: We agree that the ubiquitous seasonal acceleration is indicative of a common seasonal forcing (i.e. runoff). Annual correlations between discharge and runoff are not significant, however, likely due to the limited impact of runoff on longer term accelerations (please see the added text to Page 11, Line 21 in response to a comment from reviewer 1): “Previous work focused on land-terminating glaciated regions of the GrIS (Sundal et al 2011; Tedstone et al. 2015) and work using modeled channelization processes (Schoof 2010) demonstrated that meltwater impacts on glacier velocities operate on narrow temporal windows and may even result in a net deceleration on seasonal to annual timescales.”

We agree with the reviewer’s point on the possible difference between peak melting and peak runoff entering the margins, and note it as a consideration in the offset between runoff and discharge peaks. The temporal lag between the timing of maximum acceleration in runoff and peak *D* may be related to runoff residence time, or time it takes meltwater runoff to reach the margins of the ice sheet (noted in the last paragraph of the discussion).

Minor comments

Page 1, Line 24

remove comma after ‘variability’.

Response: Removed.

Page 1, Line 30 through Page 2, Line 3

Note that these lines may need to be revised if certain publications make it to press before this is accepted/published. The past two years have seen a remarkable slowdown in ice loss in GIS.

Response: We look forward to seeing work of mass balance estimates through present.

Page 2, Line 27

Suggest putting the phrase following (SMB) into the parens with SMB, i.e. “(SMB; the sum of the mass gained from . . .)”

Response: We have changed the text following this suggestion.

Page 6, Line 23

Do you discuss / speculate as to the cause of the second peak?

Response: We do not speculate the cause of the secondary peak at this time, although we point to two references that find the majority of contemporary acceleration at Jakobshavn to be controlled by frontal changes. We have added the following text and references to Page 6, Line 23 in the manuscript:

“We do not further investigate the cause of this secondary peak but note that previous work (Sundal et al. 2013; Bondizio et al. 2017) found that the majority of acceleration events at Jakobshavn are closely linked to changes at the calving front.”

1. Bondizio, J. H., Morlighem, M., Seroussi, H., Kleiner, T., Rückamp, M., Mouginot, J., Moon, T., Larour, E. Y. and Humbert, A.: The mechanisms behind Jakobshavn Isbræ’s acceleration and mass loss: A 3-D thermomechanical model study, *Geophys. Res. Lett.*, 44(12), 6252–6260, doi:10.1002/2017GL073309, 2017.
2. Sundal, A. V., Shepherd, A., Van Den Broeke, M., Van Angelen, J., Gourmelen, N. and Park, J.: Controls on short-term variations in Greenland glacier dynamics, *J. Glaciol.*, 59(217), 883–892, doi:10.3189/2013JoG13J019, 2013.

Page 7, Line 26

Suggest ‘As noted before, there is. . .’

Response: Changes applied.

Other author amendments

We added the following text for improved clarity on Page 8, Line 12:

“Note that the GrIS-wide weighted front position totals do not include 79 North Glacier and Zachariæ Isstrøm for reasons described in Section 2, and thus the discharge contributions of those two glaciers are excluded from the annual D term.”

We changed Figure S2 to only show one example, rather than two, in order to improve the readability of figure details.

Seasonal to decadal variability in ice discharge from the Greenland Ice Sheet

Michalea D. King^{1,2}, Ian M. Howat^{1,2}, Seongsu Jeong³, Myoung J. Noh¹, Bert Wouters^{4,5}, Brice Noël⁴, and Michiel R. van den Broeke⁴

5 ¹Byrd Polar and Climate Research Center, Columbus, USA.

²School of Earth Sciences, Ohio State University, Columbus, USA.

³Department of Earth System Science, University of California, Irvine

⁴Institute for Marine and Atmospheric research Utrecht, Utrecht University, Utrecht, Netherlands.

⁵Faculty of Civil Engineering and Geosciences, Delft University of Technology, Delft, Netherlands

10

Correspondence to: Michalea D. King (michaleaking@gmail.com)

Abstract. Rapid changes in thickness and velocity have been observed at many marine-terminating glaciers in Greenland, impacting the volume of ice they export, or discharge, from the ice sheet. While annual estimates of ice-sheet wide discharge have been previously derived, higher-resolution records are required to fully constrain the temporal response of these
15 glaciers to various climatic and mechanical drivers that vary in sub-annual scales. Here we **sample outlet glaciers wider than 1 km (N = 230) to** derive the first continuous, ice-sheet wide record of total ice sheet discharge for the **2000–2016 period**, resolving a seasonal variability of 6 %. The amplitude of seasonality varies spatially across the ice sheet from 5 % in the southeastern region to 9 % in the northwest region. We analyze seasonal to annual variability in the discharge time series with respect to both modelled meltwater runoff, obtained from RACMO2.3p2, and glacier front position changes over the
20 same period. We find that year-to-year changes in total ice sheet discharge are related to annual front changes ($r^2 = 0.59$, $p = 10^{-4}$) and that the annual magnitude of discharge is closely related to cumulative front position changes ($r^2 = 0.79$), which show a net retreat of > 400 km, or an average retreat of > 2 km at each surveyed glacier. Neither maximum seasonal runoff or annual runoff totals are correlated to annual discharge, which suggests that larger annual quantities of runoff do not relate to increased annual discharge. Discharge and runoff, however, follow similar patterns of seasonal variability with near-
25 coincident periods of acceleration and seasonal maxima. These results suggest that changes in glacier front position drive secular trends in discharge, whereas the impact of runoff is likely limited to the summer months when observed seasonal variations are substantially controlled by the timing of meltwater input.

1 Introduction

Mass loss from the Greenland Ice Sheet (GrIS) is now the single largest cause of sea level rise (Vaughan et al. **2013; AMAP**
30 **2017**), contributing approximately 1 mm a^{-1} of global water equivalent over the 2010–2015 period (van den Broeke et al. 2016). Since the mid 1990's, the GrIS has been losing ice at an increasing rate (Rignot et al. 2011; Sasgen et al. 2012; Hanna

et al. 2013; Enderlin et al. 2014) due in part to increased discharge from marine-terminating outlet glaciers (Rignot and Kanagaratnam, 2006; Rignot et al. 2008; Enderlin et al. 2014; Andersen et al. 2015). Substantial increases in ice discharge are observed at large outlet glaciers over periods of months or less (e.g. Joughin et al., 2004; Howat et al. 2005), demonstrating short term sensitivity to external drivers, such as ocean circulation (Straneo et al. 2013; Walsh et al. 2012) melt runoff (Joughin et al. 2008; Andersen et al. 2011), and sea ice/mélange conditions near the calving front (Howat et al. 2010; Carr et al. 2013; Moon et al. 2015; Bendtsen et al. 2017). Thus, understanding the dynamics of these glaciers requires measurements with a high temporal resolution.

Seasonal variability in the flow speed of marine-terminating glaciers in Greenland has been observed for small samples of glaciers (Howat et al. 2010; Howat et al. 2011; Hill et al. 2018) and for larger glacier inventories over short time periods (Howat et al. 2008; Moon et al. 2014; Moon et al. 2015). Previous ice sheet-wide estimates of discharge were largely based on summertime velocities and, therefore, may be biased toward higher values, demonstrating the need for decadal records of ice sheet-wide discharge that resolves seasonal to sub-monthly variability, potentially associated with surface meltwater runoff and calving. Here we present the first continuous record of daily estimates of net ice sheet discharge, derived over the 2000–2016 period. This record is used to resolve both distinct ice-sheet wide and regional patterns of seasonal variability and evaluate how seasonality has changed through time. We then compare these records to modelled meltwater runoff data and records of glacier front positions to assess how these terms impact discharge on seasonal to annual time scales.

2 Data and Methods

Following Howat et al. (2011), we derive time series of the rate of solid ice discharge (D) for 230 glaciers (Figure S4) with widths greater than 1 km by integrating the product of glacier thickness, ice velocity, and ice density across the glacier width at the grounded terminus. Observations are sampled along a static profile, i.e. fluxgate, oriented perpendicular to the direction of flow and located upstream of the grounding line, immediately inland of the most retreated grounding line during the 2000–2016 study period. We use the same flux gates as Howat et al. (2011) and Enderlin et al. (2014) except in cases where the grounding line had retreated inland of the gate location. Further, while Enderlin et al. (2014) used empirical relationships to estimate cross-sectional area and discharge at glaciers for which only along-flow profiles or no bed topography were available, we use the BedMachine version 3 gridded bed topography dataset (Morlighem et al. 2017), which uses ice thickness, flow speed observations and surface mass balance (SMB, i.e. the sum of the mass gained from accumulation and lost due to meltwater runoff, sublimation and snow drift erosion) to constrain a mass conservation model. As in prior studies, we assume that changes in the elevation of the glacier bed, due to erosion, deposition and/or lithosphere displacement, are small, as are variations in ice flow velocity with depth in fast flowing ($> 1 \text{ km a}^{-1}$) glaciers. Bed topographic errors across our sampled flux gates average $70 \pm 52 \text{ m}$. Thus, discharge is estimated from the bed topography and repeat measurements of surface elevation, the difference of which provides the time-variable ice thickness, and ice flow

velocity. Additional information regarding the placement of flux gates and descriptions of the datasets are provided in the supplementary material.

Enderlin et al. (2014) derived annual discharge estimates from velocity data that were mostly collected between April and September. Increased data collection by SAR sensors (Terra/TandemSAR-X), low-light level functionality of Landsat 8 (Jeong and Howat, 2015; Fahnestock et al. 2016), and increased sampling density using image pairs between multiple sensors and/or acquired from crossing orbital tracks (Rosenau et al. 2015; Jeong et al. 2017), enable substantially better temporal resolution than available for Enderlin et al. (2014). Thus, we combine this increased velocity sampling with a Kalman filter approach to estimate D and its uncertainty as a continuous series. For each glacier, we first derive a standard seasonality curve by detrending the time series of monthly mean speeds and grouping mean speeds by the month of year, so that a 17-year time series would provide up to 17 estimates of mean speed for a given month. The standard seasonality is then obtained from the median value and covariance of the observations for each month and represents a “typical” pattern of change at each respective glacier. Months with fewer available observations will therefore tend to have a higher range of uncertainty. If no optical or radar data exist for a particular month throughout the time series, a standard monthly value is estimated by fitting a periodic function to the available monthly median values. The periodicity described here does not indicate that a symmetric, sinusoidal seasonality is assumed, but rather that by detrending the time series and isolating a mean seasonal pattern of change, we expect the endpoints of the curve to be the same (i.e. the 12-month curve would repeat). The seasonality curve is then normalized to yield an estimate of fractional change in speed between months, which informs a simple linear model. Within the Kalman filter framework, this linear model assimilates the observations to optimize estimates for missing months of the time series, with the errors equal to the combination of the observation and prediction errors. Uncertainty in the seasonality curves tend to exceed observational errors, resulting in formal errors that increase with distance from the observations. A more detailed description of this approach is provided in the supplementary material. Velocity measurements for the four northernmost glaciers (Steenby, C.H. Ostenfeld, Academy, and Hagen Brae) and several small glaciers near the central eastern margin were too sparse to derive a continuous time series and we instead estimate an annual D for these glaciers. This data sparsity occurs when months of missing data exceed the number of months containing reliable observations post-filtering, preventing a resolvable seasonality.

We use the same repeat ice surface elevation dataset as Enderlin et al. (2014), extended through 2016, and with the addition of stereoscopic digital elevation models produced from sub-meter resolution DigitalGlobe Inc. WorldView imagery for the ArcticDEM project (www.arcticdem.org). The DEMs are produced to 2 m resolution and coregistered over stationary (exposed rock) surfaces using the algorithm of Noh and Howat (2014). Following coregistration to remove biases, these data have an accuracy of better than ± 0.5 m (Noh and Howat, 2015). Elevation profiles are filtered for noise and smoothed as described in the supplementary material before subtracting the BedMachine V3 bed profiles from each surface elevation profile to give ice thicknesses. The series of ice thickness estimates were then linearly interpolated to the times of the series

of velocity observations to obtain ice discharge rate, D . Errors in discharge at velocity observation times are calculated from propagation of measurement errors and uncertainties of interpolated values are determined from a Monte Carlo ensemble, as described in the supplementary material. We derive total ice sheet mass balance over the 2000–2016 period by combining our estimates of D with SMB data obtained a 5.5 km simulation of the Regional Atmospheric Climate Model, RACMO2.3 version 2 (RACMO2.3p2) statistically downscaled to 1 km, and compare these totals to monthly satellite gravimetry observations of ice sheet mass balance from the Gravity Recovery and Climate Experiment (GRACE). While RACMO2.3p2 applies the same model physics as described in Noël et al. (2018), a twice finer horizontal resolution (5.5 km instead of 11 km) better resolves SMB gradients over narrow glaciers at the ice sheet margins. Based on comparison with observations, the uncertainty in modelled basin-integrated runoff and snow accumulation (total precipitation minus sublimation) are, respectively, 20 % and 10%, which are combined to obtain an uncertainty in SMB by assuming the two are independent of each other (Noël et al., 2018; Van As et al., 2018).

We examine how D varies in response to meltwater runoff and changes glacier front position. Daily meltwater runoff estimates are also obtained from the RACMO2.3p2 product. Daily runoff values at each model grid point are summed over the ice sheet and within regional basins for comparison to D . We measure relative changes in glacier front position manually for the period 2000–2016 using all available imagery from ASTER and LANDSAT 4–8. This resulted in a measurement frequency of up to every few days during the summer, declining in frequency during the polar night, especially prior to 2012 (Landsat 8 launch). Due to the very large quantity of measurements, we used the efficient centerline methodology described in Walsh et al. (2012), who found a negligible difference in the temporal variation of front position between this and methods that involve digitization of the entire front. To enable comparison with discharge and runoff time series, we convert the irregular front position observations to daily rates of change and then resample the rates at 7-day intervals. The new resampled subset is then linearly interpolated to daily rates of front position change over the study period. Individual glacier records of frontal change are combined into regional and GrIS-wide records by first applying a discharge-dependent weighting function, so that retreat and advance events at larger glaciers are weighted more heavily, due to the proportionally larger impact of these glaciers on the discharge time series. We do not include front position measurements for Zachariae Isstrøm and 79 North Glacier because the perennial mélange of tabular icebergs at their fronts make delineation of the front position arbitrary (e.g. Moon et al. 2008).

3 Results

3.1 Net Ice Sheet Discharge and Mass Balance

The net GrIS-wide D reveals a clear seasonality, typically characterized by an annual minimum in December and a maximum in mid-July (Figure 1), superimposed upon multi-year variability. Removing the linearly-interpolated annual

means from the time series gives an average seasonal amplitude of 30 Gta^{-1} , or approximately 6 % of the mean annual discharge. The seasonal amplitude was largest in 2002, 2004, and 2005, reaching up to 46 Gta^{-1} , and, on average, higher before 2005 ($35 \pm 8 \text{ Gta}^{-1}$, where the uncertainty is $1-\sigma$). This compares to an average seasonal amplitude of $27 \pm 4 \text{ Gta}^{-1}$ after 2006, with overall trend of -0.7 Gta^{-1} from 2000 to 2016. Beginning from a mean annual discharge of $440 \pm 8 \text{ Gta}^{-1}$ in 2000, D increases to a maximum of $524 \pm 9 \text{ Gta}^{-1}$ in late June 2005, primarily due to the accelerations of Kangerdlugssuaq and Helheim glaciers in the east (Howat et al. 2007; Joughin et al. 2008). In the following two years, the rapid decrease in D from these two glaciers resulted in the greatest seasonal decrease in GrIS D in 2006, declining to a minimum of $461 \pm 9 \text{ Gta}^{-1}$ by January 2008. D then gradually increased, reaching the second-highest time series annual maximum of $494 \pm 6 \text{ Gta}^{-1}$ in 2015, with a peak summertime value of $511 \pm 6 \text{ Gta}^{-1}$ in July 2015. Annual D declined by 5 Gta^{-1} in 2016 largely due to reductions in discharge observed at Køge Bugt and Jakobshavn (Figure S3). Thus, D has remained consistently between 10 to 12 % above the 2000 rates since 2010. Along with the annual mean quantities, the seasonal discharge signal varies throughout the study period. Prior to 2013, the seasonal variation in D is relatively symmetric, with a single distinct peak and little variability on sub-annual timescales. The final four years of the record are more variable, with minor peaks following the seasonal maxima. This pattern is predominantly due to changes observed in the NW region, addressed in detail in Sect. 3.2.

The ice sheet's 20 largest glaciers account for over 50 % of the total D (Figure S4). Of these 20, the four largest glaciers (Fig. S3) together account for 25 % of the total D , and 56 % of the cumulative anomaly in GrIS-wide D relative to annual D in 2000. Variations in these four glaciers, therefore, dominate variability in total GrIS D . The secular trend of the combined D is substantially different with the four largest glaciers removed (Figure S5). Following the decline in D between 2005 and 2008, the combined D of the remaining glaciers, denoted here as D_s , continued to increase, reaching a maximum in 2011 before declining to another minimum 2012. The seasonal decline in D_s during the winter of 2013–2014 was anomalously reduced relative to other years, with speeds remaining elevated across the ice sheet. D_s then increased to a record maximum in July 2015, reaching an annual maximum of $374 \pm 5 \text{ Gta}^{-1}$ in 2016. Thus, an overall continued increase in D_s since 2008 was largely offset in declines from the four largest glaciers over that period. Removing the four largest glaciers, however, does not change the relative seasonal amplitude of approximately 6 %, indicating that GrIS-wide seasonality is not dependent on the largest glaciers.

Our continuous estimates of D enable the first direct comparison to monthly satellite gravimetry observations of ice sheet mass balance from GRACE. We compute ice sheet mass balance by subtracting our estimates of net GrIS-wide D from daily 1 km^2 resolution SMB estimates obtained from RACMO2.3p2 (Noël et al., 2018). Following the methodology of van den Broeke et al. (2016), we incorporate SMB fluxes from the ice-free tundra and peripheral ice caps, which are included in the GRACE signal, into the ice-sheet mass balance calculations. Mass balance estimates of peripheral ice caps derived from laser altimetry (Bolch et al. 2013) found that areal averaged mass losses were similar for land-terminating and marine-

terminating glaciers, and thus we assume D from peripheral glaciers and ice caps is small relative to the errors in other terms. We remove the SMB over ice shelves, downstream of the discharge flux gates, from the total. We use GRACE ice sheet mass updated from Wouters et al. (2013), corrected for glacial isostatic adjustment using the model of Khan et al. 2016. The cumulative mass losses estimated by $SMB - D$ and GRACE, calculated by taking the difference between the annual mean cumulative losses in 2016 and 2003, are 3263 ± 259 and 3479 ± 280 Gt, respectively, over the 2003–2016 period (Figure 2). This 7% difference equates to an integrated monthly bias of less than 1.5 Gt, nearly all of which is due to a greater loss estimated by GRACE in the anomalously severe 2011 and 2012 melt seasons. Extended to the beginning of the D time series, we estimate a total cumulative mass loss from 2000 through 2016 of 3730 ± 277 Gt. We also delineate individual glacier D records and SMB totals to align with the six regional basins used in Wouters et al. (2013) and compare these quantities to basin-scale GRACE estimates (Table 1, and Figures S6, S7). We find that while the seasonal variability in mass loss shown in GRACE is well resolved by $SMB - D$ estimates for all basins, the level of agreement in magnitude of cumulative mass loss varies by basin. Estimates agree within their combined uncertainty ($< \pm 10 \text{ Gt a}^{-1}$) for three basins, which together account for $\sim 65\%$ of the total mass loss. Annual mass loss rates from $SMB - D$ in Basin 1 and 2 (northern regions) exceed GRACE estimates rates by more than 50%, and mass loss rates from GRACE are approximately double those from $SMB - D$ in Basin 4 (southeast). These differences largely cancel each other out, leading to the close agreement between estimates for the GrIS as a whole.

3.2 Regional Discharge Variability

Partitioning D into the four quadrants used by Enderlin et al. (2013), we find significant spatial variability (Figure 3a), with regional D quantities summarized in Table 2. The northwestern (NW) region, which includes Jakobshavn northward to and including Petermann Glacier, has the highest combined discharge, averaging 207 Gt a^{-1} , with a cumulative discharge anomaly, defined as the cumulative difference from the year 2000 D , of 343 ± 21 Gt. In the NW, we also find the highest seasonal amplitude in D of $18 \pm 3 \text{ Gt a}^{-1}$ or 9%, with Jakobshavn Glacier (Figure S3A) alone contributing $7 \pm 3 \text{ Gt a}^{-1}$. Removing this glacier from the sample reduces the fractional seasonal amplitude to the GrIS-wide average of 6% ($10 \pm 1.7 \text{ Gt a}^{-1}$). On average, maximum D occurs on 12 July (day 192) with a uniform, sinusoidal seasonal cycle transitioning to an irregular, saw tooth pattern in 2012. This shift is also visible in the GrIS-wide time series and is primarily due to the emergence of a secondary, mid to late autumn peak in D at Jakobshavn (Figure S3A). We do not further investigate the cause of this secondary peak but note that previous work (Sundal et al. 2013; Bondizo et al. 2017) found that the majority of acceleration events at Jakobshavn are closely linked to changes at the calving front. On average, D at Jakobshavn reaches a seasonal maximum ~ 1 week later than the NW regionally averaged maxima. We find no significant trend in the timing of the seasonal maximum in the NW.

The southeastern (SE) region, extending northward to and including Kangerdlugssuaq glacier, had a cumulative D anomaly of 284 ± 17 Gt since 2000 (Figure 3b). Approximately 60 % of the cumulative anomaly occurred at Helheim and Kangerdlugssuaq, due to the rapid 2004–2005 terminus retreat and subsequent acceleration (Howat et al. 2007), resulting in the SE reaching a period maximum rate of D of 238 ± 4 Gta⁻¹ in June 2005. Following this period of acceleration, regional D values steadily declined to an annual average of 187 ± 4 Gta⁻¹ in 2016, within the error of D observed in 2000 (182 ± 6 Gta⁻¹), prior to acceleration. As discovered by Enderlin et al. (2014), an overall decreasing trend in SE D of -1.7 Gta⁻² after 2005 has partially offset the overall increase of 2.7 Gta⁻² in the NW. Despite a large net regional D , there is substantially less seasonal variation in the SE, with an average seasonal amplitude of 9 ± 5 Gta⁻¹ or 5 %. The seasonal amplitude was greater during the 2000–2005 period of acceleration (14 ± 6 Gta⁻¹) than during the 2006–2016 period (7 ± 2 Gta⁻¹). The three largest glaciers in this region (Køge Bugt, Helheim, and Kangerdlugssuaq) together contribute approximately 40 % of the net regional D . A seasonal signal is more visible after 2005 when excluding these three glaciers, with the remaining glaciers showing a slightly larger seasonal amplitude of approximately 6 %. On average, the summertime seasonal maxima in D occur approximately one week earlier in the SE than in the NW.

The NE and SW regions have fewer marine terminating outlet glaciers and contribute less to the total GrIS D . Discharge from the northeast (NE) region (Figure 3c), contributes approximately 12 % of the total ice sheet D , with the regional ice flux dominated by Zachariæ Isstrøm and 79 North Glacier. This region exhibits a relatively consistent seasonal variability of 5 ± 1 Gta⁻¹, or 8 %. The seasonal maximum typically occurs at the end of June. Annual D increased by 4 Gta⁻¹ between 2013 and 2016, largely due to increased D observed at Zachariæ Isstrøm (Mouginot et al. 2015; Choi et al. 2017). D in the NE shows a steady increase, accelerating from a rate of ~ 0.2 Gta⁻² during 2000–2012 to over 1 Gta⁻² during the 2013–2016 period, entirely due to acceleration of Zachariæ Isstrøm and 79 North glaciers. Lastly, only 7 glaciers constitute the southwest (SW) (Figure 3d), where land-terminating glaciers dominate the margin. Kangia glacier alone accounts for over approximately 60 % of the total SW regional D . A doubling of the seasonal amplitude at Narssap Glacier, coinciding with rapid terminus retreat (Motyka et al. 2017), is responsible for the increase in regional variability after 2011.

As mentioned above, variations in D may be due primarily to the largest glaciers, which may or may not represent typical glacier behavior. To assess seasonal glacier dynamics, we remove the impact of glacier size by first subtracting the secular trend from the series and then normalizing each glacier's detrended D series by its maximum seasonal amplitude. This process effectively creates equally-weighted time series of D for individual glaciers, while isolating the seasonal signal. The averages of the normalized seasonal discharge for each region and the total GrIS are shown in Figure 4 and reveal that a distinct seasonal signal is a ubiquitous feature across the ice sheet, independent of glacier size. However, the timing of the seasonal maxima in the normalized data occurs approximately ten days earlier (late June, typically) than without normalization. As noted above, there is also a decrease in seasonal amplitude since 2013 of 20 % relative to earlier years. We observe a similar decrease in amplitude in the normalized series for the SE, NW and NE. This widespread reduction in

seasonal amplitude corresponds with a period of relatively stable mean annual D , as shown in Fig. 1. As was noted from the raw regional D , the SE region exhibits the smallest seasonal variability. Unlike the raw time series, which showed the greatest seasonal amplitude in the NW, the NE region shows the largest seasonal amplitude in the normalized time series. This is likely due to the reduced impact of Jakobshavn on NW seasonality through the normalization. Fig. 4 also shows that the seasonal maxima occur coincidentally for the majority of glaciers over the majority of the GrIS, with the few glaciers in the SW reaching a seasonal maximum slightly earlier than the GrIS-wide average.

3.3 Variations in Annual Discharge, Front Position and Runoff

We expect that D will vary with both ice front position, due to changes in resistive stress at the terminus (e.g. Thomas et al. 2004; Howat et al. 2008), and with seasonal meltwater runoff, due to variations in basal water pressure (e.g. Joughin et al., 2012). We first test for broad, linear correlations between annual discharge, both over the entire GrIS and regionally, and annual changes in front position and total runoff. We calculate the GrIS-wide and regional annual runoff totals from daily RACMO2.3p2 outputs. Ice sheet-wide and regional front positions are the sum of each glacier's change between 1 January each year, weighted by the fractional contribution of the glacier's D to the GrIS or regional total. We then divide these sums by the total number of glaciers across the GrIS or region of interest and express the quantity as the mean weighted position change.

For the entire GrIS, we find the strongest relationship between annual D and the weighted, cumulative change in 1 January front position ($r^2 = 0.79$, $p = 10^{-6}$) (Figure 5A). Note that the GrIS-wide weighted front position totals do not include 79 North Glacier and Zachariæ Isstrøm for reasons described in Section 2, and thus the discharge contributions of those two glaciers are excluded from the annual D term. This correlation is slightly stronger than that obtained between annual D and the cumulative front position change from the previous year ($r^2 = 0.68$, $p = 10^{-4}$). A weaker, but significant correlation is found between the change in annual D , defined here as the difference between the current and previous year's annual D , and annual front position change during both the current year ($r^2 = 0.59$, $p = 0.0005$) (Figure 5b) and the previous year ($r^2 = 0.50$, $p = 0.002$). We test for these lagged relationships between retreat and annual D to account for the temporal grouping of the data. For example, front position may continue to retreat into the autumn, after the typical peak in D . If autumn/wintertime discharge rates remain elevated as a result of continued retreat through December of the previous year, we would anticipate the following springtime acceleration to be superimposed on a higher base discharge rate. These correlations are strengthened by excluding Petermann Glacier, where large retreats of its uniquely thin and fractured ice shelf in 2010 and 2012 had no resolvable impact on ice flow speed and, thus, D (Lemos et al. 2018; Münchow et al., 2014). In contrast, no significant correlation is found between annual D and total annual runoff. The addition of annual runoff as an independent variable also does not improve the correlations with front position described above.

Retreat was widespread over the study period in the NW, with glaciers there retreating, on average, 2.8 km from 2000 to 2016. The cumulative, weighted regional front position change shows a near-linear annual retreat with small interannual variation. A similarly strong linear trend is present in annual D , resulting in a nearly perfect correlation with annual cumulative front position change ($r^2 = 0.92$, $p = 10^{-9}$) (Figure 5c). This relationship is slightly strengthened at a one-year lag, with a correlation of $r^2 = 0.94$ ($p = 10^{-9}$) between annual D and cumulative front position up through the previous year. Only a weakly significant ($r^2 = 0.25$, $p = 0.048$) relationship exists between the change in NW annual D and the annual, rather than cumulative, front change during the previous year. Retreat also dominated in the SE region over the study period, averaging 1.7 km. Unlike in the NW, however, D in the SE correlated to the annual weighted change in front position, rather than cumulative change. Annual D is significantly correlated to the previous year's annual front position change ($r^2 = 0.28$, $p = 0.033$). Even stronger is the correlation between the change in annual D and the annual front position change of the previous year, ($r^2 = 0.60$, $p = 10^{-4}$) (Figure 5d and Figure S8). As with the complete GrIS, no significant correlations are found between D or interannual change in D and annual runoff in either the SE or NW regions.

3.4 Seasonal Variations in Discharge, Front Position and Runoff

Runoff on the ice sheet typically begins in May and continues through September, reaching a maximum daily rate in July. Smoothing daily runoff values with a monthly (31-day) running mean results in a seasonal distribution with one or several distinct peak(s). Comparing GrIS-wide D to the smoothed runoff series (Figure 6), we find that seasonal acceleration of D is greatest at the onset of runoff, and reaches a seasonal maximum, on average, 13 ± 9 days after the greatest increase in runoff and 12 ± 7 days before the seasonal maximum in runoff. The only exception to this progression was in 2013, when the peak in D occurred after the seasonal maximum in runoff. The maximum D occurs, on average, 40 ± 8 days after the onset of significant runoff. Since the distribution of daily runoff includes a long tail of small values, we define the significant runoff onset as the day when runoff exceeds the 50th percentile of daily runoff values between April 1 and November 1. We use this threshold to delineate the onset of significant runoff by separating days with negligible runoff contributions from those with non-negligible runoff contributions. We find a significant correlation between the date of runoff onset and the date of maximum D ($r^2 = 0.33$, $p = 0.015$), indicating that a later-occurring peak D may be related to later onset of runoff. However, despite the near synchronous timing between seasonal peaks in runoff and D , we find no other significant relationships between the timing of runoff and discharge, nor between the magnitude of runoff and the magnitude of the seasonal maximum D , or total annual D .

There is regional variability in the timing and amplitude of runoff. The NW region reaches an average maximum of 2.6 ± 0.5 Gt day⁻¹ on day 199 (± 8), totaling 82 ± 21 Gt annually. Significant runoff onset occurs in early June (day 160 ± 7), one week later than runoff in the SE (day 15 ± 8) and preceding the timing of the regional maximum D by approximately one month (32 ± 10 days). There is a significant relationship in the NW region between the timing of runoff onset and the timing of the

seasonal maximum in D ($r^2 = 0.46$ $p = 0.003$). In the SE, there is a similar magnitude of total annual runoff (75 ± 16 Gt), but a substantially lower maximum daily rate of 1.7 ± 0.5 Gt day⁻¹ which occurs, on average, on day 208 (± 10). There is also a greater interannual variability in the temporal separation between onset of runoff and maximum D (33 ± 22 days) in the SE region and, as a result, there is no significant correlation in their timing. As with the GrIS as a whole, we find no significant relationships between the magnitudes of runoff and D , or total annual D , in either region.

Front position also varies seasonally. Integrated over the GrIS, net weighted retreat begins in early April (day 92 ± 33) and continues through the end of September (day 265 ± 17). Daily rates of retreat increase most rapidly in early June (day 153 ± 41), reaching, on average, a maximum retreat rate on day 180 (± 35). We test for linear relationships between the timing of initial retreat and greatest increase in retreat, and timing and magnitude of maximum daily rate of retreat with the same seasonal D metrics described above (e.g. magnitude and timing of maximum D and timing of greatest increase in D). We find no significant relationships between the timing or magnitude of seasonal frontal change quantities with seasonal D . The seasonal progression of retreat and advance occurs earlier in the NW relative to the GrIS-wide average. In this region, total weighted front change rates show the greatest increase in retreat in mid-May, on average, (day 135 ± 46), and reach a peak retreat rate in mid-June (day 167 ± 38). In the SE region, by contrast, retreat accelerates the most in mid-June (day 169 ± 46) and reaches a maximum rate on day 200 (± 23). As with the GrIS-wide results, we find no significant correlations between the seasonality of retreat and D at the regional scale.

4 Discussion

Our GrIS-wide estimate of D in 2000 (440 ± 8 Gta⁻¹) is approximately 5 % and 20 % lower than annual estimates derived for 2000 in Enderlin et al. (2014) and Rignot et al. (2011), respectively. Our 2003–2010 mean D of 484 ± 9 Gta⁻¹ agrees within margins of uncertainty to estimates by Kjeldsen et al. (2015) over the same time period (465 ± 65.5 Gta⁻¹) with a bias of less than 20 Gta⁻¹. Annual D estimates for 2007 and 2011 are approximately 5 % and 7 % lower than those estimated in Andersen et al. 2015, but also within margins of uncertainty. Approximately half of the difference from Enderlin et al. (2014) can be explained by the bias resulting from the study's use of, mostly, summertime median velocities and therefore higher discharge values. Other differences are likely due to a combination of observational error, uncertainties associated with empirical assumptions made in the absence of ice thickness data, methodological differences in the processing and filtering of surface elevation data, and uncertainties associated with ice thickness derivations using hydrostatic equilibrium assumptions (Rignot et al. 2011). The higher temporal resolution of D presented here also avoids nonuniform temporal sampling biases, and, once combined with SMB data from RACMO2.3p2, is in close agreement with independent estimates of ice sheet mass balance from GRACE. Significant discrepancies, however, between the SMB – D and GRACE estimates still exist at the regional scale (Figure S6), with SMB – D predicting nearly twice the loss in north of the ice sheet, but approximately half

the loss of GRACE in the southeast. The difference in the SE may be due to an underestimation of either runoff, partly from the high slope of the ablation zone, overestimated accumulation rates, or ice thickness for glaciers lacking radio echo sounding measurements near the terminus. The differences in the north may be due to unrealistically low net SMB predicted there by RACMO2.3p2, with some years showing zero or negative SMB, and cumulative SMB loss in region 1 (Figure S7).

5

The seasonal variation in D of 6 % is significantly less than the ~ 10 % typically assumed for the GrIS (e.g. Rignot and Kanagaratnam, 2006; Andersen et al. 2015). While individual regions have larger relative seasonal variations, differences in the timing of their peaks cause them to offset each other in total. For instance, the GrIS-wide seasonal amplitude would be 60 Gta⁻¹, or nearly 13 %, if the seasonal signals expressed at individual glaciers were exactly in-phase. This effect of offsetting variability was especially strong in 2013, where early increases in D in the SE region dampened the winter minimum. The seasonal amplitude of GrIS has also declined since 2013 due to the widespread, 20 % reduction in the discharge seasonality of SE glaciers.

10

Changes in glacier discharge are due to changes in both ice flow speed and thickness, with less known about short-term (seasonal to interannual) variations in the latter. Consistent with numerous studies (e.g. Helm et al. 2014; Csatho et al. 2014; Kjeldsen et al. 2015), 89 % of the glaciers, including the 25 largest, thinned over the study period. Holding ice thickness constant, so that the change in discharge is due entirely to changes in flow speed, results in an increase in D of 110 Gta⁻¹ by 2016, or 60 Gta⁻¹ greater than estimated when including ice thickness change (Figure S9). Thus, ice thinning has offset the increase in D due to ice flow acceleration by over 50 % since 2000, and this fraction is steadily increasing with time since the initial, rapid acceleration in the SE in 2004 and 2005 (Figure S10b). Ice thickness changes on sub-annual timescales also reduce the seasonal amplitude of D . Holding thickness constant, as above, results in a seasonal variation that is, on average, 10% larger than if thickness changes are included. Thus, inclusion of ice thickness change on sub-annual to decadal timescales is essential for accurate estimates of D .

15

20

25

30

Changes in ice thickness also modulate the relationship between changes in D and ice front position. As described in Sect. 3.3, cumulative annual front change and annual D are uncorrelated in the SE region. However, holding ice thickness constant, as above, results in a strong correlation ($r^2 = 0.79$, $p = 10^{-6}$), which is similar to that in the NW. Holding ice thickness constant (Figure S10b) also increases the strength of the correlation between annual changes in front position and the change in annual D the following year ($r^2 = 0.75$, $p = 10^{-5}$). These increased correlations reflect the expected dependence of ice velocity on changes in ice front position (e.g. Howat et al. 2008; Nick et al. 2009; Vieli and Nick, 2011). The SE underwent a sudden, large increase in velocity and retreat in ice front position between 2002 and 2005, with another, smaller acceleration and retreat in 2010, but has since remained largely stable through 2016. Recent work by Bunce et al. (2018) describes increased interannual variability in SE front position, due to asynchronous retreat observed at glaciers in that region. This asynchrony may also contribute to the more recent muted seasonality in the SE region, as previously described.

While velocity has remained stable, ice thinning has resulted in a declining D that is uncorrelated with cumulative ice front retreat. In contrast, both retreat and D have been increasing steadily in the NW throughout the record, indicating steadily increasing ice speeds, resulting in a high correlation between annual D and cumulative front position change (i.e. retreat).

5 Lastly, we expect glaciers to respond to changes in basal water pressure due to the seasonal input of runoff. Previous work
focused on land-terminating glaciated regions of the GrIS (Sundal et al 2011; Tedstone et al. 2015) and work using modeled
channelization processes (Schoof 2010) demonstrated that meltwater impacts on glacier velocities operate on narrow
temporal windows and may even result in a net deceleration on seasonal to annual timescales. While both D and meltwater
10 runoff show a similar pattern of seasonal variability, with a possible relationship between the timing of the onset of runoff
and the seasonal peak in D , neither the seasonal maximum in runoff, nor the seasonally-integrated runoff, are significantly
correlated to annual D . These indicate a more complex interaction between runoff, ice flow velocity and D , where the rate
and distribution of runoff into the subglacial system are more relevant to glacier flow than total runoff (Stearns and van der
15 Veer, 2018). For example, the sensitivity of D to runoff may vary throughout the melt season, with increased sensitivity
early in the melt season when drainage channels are inefficient and unable to support the influx of runoff into the system
(Chandler et al. 2013), thus increasing water pressure at the bed and enhancing basal flow (Palmer et al. 2011; Bartholomew
et al. 2010). This is consistent with 13 ± 9 day average lag in timing between the fastest increase in runoff and the maximum
GrIS-wide D , which is close to the 18-day average “residence time” between the production of melt runoff on the ice sheet
and its transport to the margin estimated by van Angelen et al. (2014). Thus, taking this residence time into account, the
20 seasonal maximum flow speed, and therefore D , occurs near the time we would expect maximum pressurization of the
subglacial drainage system. Future work will build on these concepts by closely examining discharge rates of acceleration
and deceleration in response to the distribution of runoff throughout the melt season, giving consideration to runoff residence
times.

5 Conclusions

GrIS-wide D has remained near 490 Gt a^{-1} following a period of rapid acceleration before 2006, representing an 11 %
25 increase from 2000. This apparent stabilization, however, is due to steady or declining flow speeds and ice thinning at the
four largest glaciers, which dominate the ice sheet-wide total. Excluding these, the combined D of the remaining glaciers
increased steadily over the time period, reaching a maximum in 2016, indicating that the largest glaciers are not
representative of typical outlet glacier change. Trends in D vary regionally, increasing in the NW and NE and remaining
steady in the SE, where sustained higher flow speeds are completely offset by ice thinning and D has returned to its year
30 2000 values. In total over the GrIS, ice thinning has offset the impact of increased ice flow speeds on D by over 50 % since
2000, substantially modulating the contribution of glacier dynamics on mass loss.

We find that annual changes in GrIS D can be mostly attributed to the cumulative, weighted change in glacier front position. This relationship is the strongest in the NW region, where continuous retreat has accompanied a near-linear increase in annual D and, therefore, changes in D are driven by changes in flow speed. In the SE, however, where speeds have remained relatively stable since 2005 while the glaciers have thinned, it is instead the annual changes in front position that correlate to changes in annual D the following year. In contrast, we find no correlations between annual D , or year-to-year changes in D , and modelled meltwater runoff. These results indicate that multi-year changes in D are dominated by changes in ice front position, through its impact to glacier dynamics, and that the magnitude of meltwater runoff has no consistent, discernible effect on total annual outlet glacier discharge.

10 We resolve a persistent, ubiquitous seasonal increase in D averaging 6 %. Regionally, this signal varies from 5 % in the SE to 9 % in the NW, with \pm 1-month differences in timing resulting in an offsetting effect that decreases the combined total. There was also a marked decline in seasonality after the period of rapid ice flow accelerations in the SE, resulting in a \sim 23 % decrease in seasonality after 2006, and a near complete disappearance of a seasonal signal in the SE after 2013. While not correlated on an annual basis, seasonal variations in D do correspond to those of runoff. We observe that maximum D

15 occurs \sim 2 weeks after maximum increases in runoff, which is similar to the expected time for runoff to reach the margin, and \sim 2 weeks before the seasonal maximum runoff. We also observe significant correlation between the onset of runoff and the timing of peaks in D , with earlier-occurring runoff onset corresponding to earlier peaks in D . This is consistent with the expected impact of increasing meltwater input to an inefficient subglacial drainage system at the start of the melt season, increasing the subglacial water pressure and glacier sliding velocity. This is followed by a decline in D before the peak in

20 runoff is reached, attributed to the transition to efficient subglacial drainage. Such a transition also may explain the lack of correlation between the magnitudes of seasonal runoff and maximum D . Thus, while changes in front position, and their resulting persistent changes to the balance of forces at the glacier terminus, appear to dominant multi-year variability in regional and total GrIS D , seasonal variations are substantially controlled by the timing of meltwater input.

25 We have assessed the bulk behavior of ice sheet discharge and its broad relationships to possible external forcing, enabled by this first, complete estimate of continuous D over nearly two decades for all of Greenland's large marine terminating glaciers. It is well established, however, that the behavior of glaciers in close proximity and under similar environmental forcing can vary substantially (e.g. McFadden et al. 2011; Moon et al. 2012; Carr et al. 2017). This is likely due to the sensitivity of outlet glacier dynamics to their particularly geometry (e.g. Enderlin et al. 2013; Porter et al. 2014; Carr et al.

30 2015; Bartholomaus et al. 2016; Catania et al. 2018) and we do not attempt to account for these differences here. However, detailed analysis of the relationships between particular glacier characteristics and their dynamics at a range of time scales using these data will be the subject of future work.

Author Contribution

MDK and IMH conceived this study and synthesized the required data sets. MDK performed the analyses and led writing the manuscript. SJ developed the orthorectified velocity maps and MJN developed algorithms for surface elevation, both used to derive the ice discharge estimations. BW processed and provided mass balance estimates derived from GRACE observations, and BN and MRB developed the surface mass balance model, RACMO2.3p2, which was combined with discharge estimates to derive an ice sheet-wide record of mass balance. All authors contributed thoughtful discussions and insights to the study, and all authors contributed to editing the manuscript.

10

Acknowledgements

This work was supported by grants 80NSSC18K1027 and NNX13AI21A from the U.S. National Aeronautics and Space Administration and a fellowship from the Ohio State University. BW was funded by NOW VIDI grant 016.Vidi.171.065.

Competing interests

The authors declare that they have no conflict of interest.

Data availability

All ice velocity and topographic products are publically available online. The velocity data maps and GIMP DEM are distributed through the NASA Distributed Active Archive Center at the NSIDC (<http://nsidc.org/data/measures/gimp>). Bed topography can also be accessed through the NSIDC portal at <https://nsidc.org/data/idbmg4>. Information on the RACMO2.3p2 SMB data can be found at <http://www.projects.science.uu.nl/iceclimate/models/greenland.php>.

25

References


- Andersen, M. L., Nettles, M., Elosegui, P., Larsen, T. B., Hamilton, G. S. and Stearns, L. A.: Quantitative estimates of velocity sensitivity to surface melt variations at a large Greenland outlet glacier, *J. Glaciol.*, 57(204), 609–620, doi:10.3189/002214311797409785, 2011.
- 5 Bartholomew, I., Nienow, P., Mair, D., Hubbard, A., King, M. A. and Sole, A.: Seasonal evolution of subglacial drainage and acceleration in a Greenland outlet glacier, *Nat. Geosci.*, 3, 408–411, doi:10.1038/ngeo863, 2010.
- 10 Bartholomew, T. C., Stearns, L. A., Sutherland, D. A., Shroyer, E. L., Nash, J. D., Walker, R. T., Catania, G., Felikson, D., Carroll, D., Fried, M. J., Noël, B. P. Y. and Broeke, M. R. V. A. N. D. E. N.: Contrasts in the response of adjacent fjords and glaciers to ice-sheet surface melt in West Greenland, *Ann. Glaciol.*, 57(73), 25–38, doi:10.1017/aog.2016.19, 2016.
- 15 Bendtsen, J., Mortensen, J., Lennert, K., Jens, K. E., Boone, W., Galindo, V., Hu, Y., Dmitrenko, I. A., Kirillov, S. A., Kjeldsen, K. K., Kristoff, Y., Barber, D. G. and Rysgaard, S.: Sea ice breakup and marine melt of a retreating tidewater outlet glacier in northeast Greenland (81 ° N), *Nature*, 1–11, doi:10.1038/s41598-017-05089-3, 2017.
- Bolch, T., Sandberg Sørensen, L., Simonsen, S. B., Mölg, N., MacHguth, H., Rastner, P. and Paul, F.: Mass loss of Greenland's glaciers and ice caps 2003-2008 revealed from ICESat laser altimetry data, *Geophys. Res. Lett.*, 40(5), 875–881, doi:10.1002/grl.50270, 2013.
- 20 Bondzio, J. H., Morlighem, M., Seroussi, H., Kleiner, T., Rückamp, M., Mougintot, J., Moon, T., Larour, E. Y. and Humbert, A.: The mechanisms behind Jakobshavn Isbræ's acceleration and mass loss: A 3-D thermomechanical model study, *Geophys. Res. Lett.*, 44(12), 6252–6260, doi:10.1002/2017GL073309, 2017.
- 25 Box, J., Sharp, Ma.: 2017. Changes to Arctic land ice. In: *Snow, Water, Ice and Permafrost in the Arctic (SWIPA) 2017. Arctic Monitoring and Assessment Programme (AMAP), Oslo, Norway, 148–168, 2017.*
- Bunce, C., Carr, J. R., Nienow, P. W., Ross, N. and Killick, R.: Ice front change of marine-terminating outlet glaciers in northwest and southeast Greenland during the 21st century, *J. Glaciol.*, 64(246), 523–535, doi:10.1017/jog.2018.44, 2018.
- 30 Carr, J. R., Vieli, A. and Stokes, C.: Influence of sea ice decline, atmospheric warming, and glacier width on marine-terminating outlet glacier behavior in northwest Greenland at seasonal to interannual timescales, *J. Geophys. Res. Earth Surf.*, 118(3), 1210–1226, doi:10.1002/jgrf.20088, 2013.

- Carr, J. R., Vieli, A., Stokes, C. R., Jamieson, S. S. R., Palmer, S. J., Christoffersen, P., Dowdeswell, J. A., Nick, F. M., Blankenship, D. D. and Young, D. A.: Basal topographic controls on rapid retreat of Humboldt Glacier, northern Greenland, *J. Glaciol.*, 61(225), 137–150, doi:10.3189/2015JoG14J128, 2015.
- 5 Carr, J. R., Stokes, C. R. and Vieli, A.: Threefold increase in marine-terminating outlet glacier retreat rates across the Atlantic Arctic: 1992–2010, *Ann. Glaciol.*, 58(74), 1–20, doi:10.1017/aog.2017.3, 2017.
- Catania, G. A., Stearns, L. A., Sutherland, D. A., Fried, M. J., Bartholomew, T. C., Morlighem, M., Shroyer, E. and Nash, J.: Geometric Controls on Tidewater Glacier Retreat in Central Western Greenland, *J. Geophys. Res. Earth Surf.*, 123(8), 2024–2038, doi:10.1029/2017JF004499, 2018.
- 10 Chandler, D. M., Wadham, J. L., Lis, G. P., Cowton, T., Sole, A., Bartholomew, I., Telling, J., Nienow, P., Bagshaw, E. B., Mair, D., Vinen, S. and Hubbard, A.: Evolution of the subglacial drainage system beneath the Greenland Ice Sheet revealed by tracers, *Nat. Geosci.*, 6, 195–198, doi:10.1038/ngeo1737, 2013.
- 15 Choi, Y., Morlighem, M., Rignot, E., Mouginot, J., and Wood, M.: Modeling the Response of Nioghalvfjærdsfjorden and Zachariæ Isstrøm Glaciers, Greenland, to Ocean Forcing Over the Next Century, *Geophys. Res. Lett.*, 44, 11, 11–71, 79, doi:10.1002/2017GL075174, 2017.
- 20 Csatho, B. M., Schenk, A. F., van der Veen, C. J., Babonis, G., Duncan, K., Rezvanbehbahani, S., van den Broeke, M. R., Simonsen, S. B., Nagarajan, S., and van Angelen, J. H.: Laser altimetry reveals complex pattern of Greenland ice sheet dynamics, *P. Natl. Acad. Sci. USA*, 111, 18478–18483, 2014.
- van As, D., Hasholt, B., Ahlstrøm, A. P., Box, J. E., Cappelen, J., Colgan, W., Fausto, R. S., Mernild, S. H., Mikkelsen, A. B., Noël, B. P. Y., Petersen, D. and van den Broeke, M. R.: Reconstructing Greenland Ice Sheet meltwater discharge through the Watson River (1949–2017), *Arctic, Antarct. Alp. Res.*, 50(1), S100010, doi:10.1080/15230430.2018.1433799, 2018.
- 25 Enderlin, E. M., Howat, I. M., Jeong, S., Noh, M. J., Angelen, J. H. van, and van den Broeke, M. R.: An improved mass budget for the Greenland ice sheet, *Geophys. Res. Lett.*, 41, 1–7, doi.org/10.1002/2013GL059010, 2014.
- 30 Enderlin, E. M., Howat, I. M. and Vieli, A.: High sensitivity of tidewater outlet glacier dynamics to shape, *The Cryosphere*, doi:10.5194/tc-7-1007-2013, 2013.

- Fahnestock, M., Scambos, T., Moon, T., Gardner, A., Haran, T., and Klinger, M.: Rapid large-area mapping of ice flow using Landsat 8, *Remote Sens. Environ.*, 185, 84–94, doi.org/10.1016/j.rse.2015.11.023, 2016.
- Hanna, E., Navarro, F. J., Pattyn, F., Domingues, C. M., Fettweis, X., Ivins, E. R., Nicholls, R. J., Ritz, C., Smith, B.,
5 Tulaczyk, S., Whitehouse, P. L., and Zwally, H. J.: Ice-sheet mass balance and climate change, *Nature*, 498, 51–59, 2013.
- Helm, V., Humbert, A., and Miller, H.: Elevation and elevation change of Greenland and Antarctica derived from CryoSat-2, *The Cryosphere*, 8, 1539–1559, doi:10.5194/tc-8-1539-2014, 2014.
- 10 Hill, E. A., Carr, J. R., Stokes, C. R. and Gudmundsson, G. H.: Dynamic changes in outlet glaciers in northern Greenland from 1948 to 2015, *The Cryosphere*, 12, 3243–3263, doi.org/10.5194/tc-12-3243-2018, 2018.
- Horgan, H. J., Anderson, B., Alley, R. B., Chamberlain, C. J., Dykes, R., Kehrl, L. M. and Townend, J.: Glacier velocity variability due to rain-induced sliding and cavity formation, *Earth Planet. Sci. Lett.*, doi:10.1016/j.epsl.2015.10.016, 2015.
15
- Howat, I. M., Joughin, I., Tulaczyk, S., and Gogineni, S.: Rapid retreat and acceleration of Helheim Glacier, east Greenland, *Geophys. Res. Lett.*, 32, L22502, doi:10.1029/2005GL024737, 2005.
- Howat, I. M., Joughin, I. and Scambos, T. A.: Rapid changes in ice discharge from Greenland outlet glaciers, *Science*,
20 3151559–61, doi:10.1126/science.1138478, 2007.
- Howat, I. M., Joughin, I., Fahnestock, M., Smith, B. E., and Scambos, T. A.: Synchronous retreat and acceleration of southeast Greenland outlet glaciers 2000–06: ice dynamics and coupling to climate, *J. Glaciol.*, 54, 646–660, doi:10.3189/002214308786570908, 2008.
25
- Howat, I. M., Box, J. E., Ahn, Y., Herrington, A., and McFadden, E. M.: Seasonal variability in the dynamics of marine-terminating outlet glaciers in Greenland, *J. Glaciol.*, 56, 601– 613, doi.org/10.3189/002214310793146232, 2010.
- Howat, I. M., Ahn, Y., Joughin, I., van den Broeke, M. R., Lenaerts, J. T. M., and Smith, B.: Mass balance of Greenland’s
30 three largest outlet glaciers, 2000–2010, *Geophys. Res. Lett.*, 38, L12501, doi:10.1029/2011GL047565, 2011.
- Howat, I. M., Negrete, A., and Smith, B. E.: The Greenland Ice Mapping Project (GIMP) land classification and surface elevation data sets, *The Cryosphere*, 8, 1509–1518, doi.org/10.5194/tc-8-1509-2014, 2014.▲

- Jeong, S., Howat, I. M. and Ahn, Y.: Improved Multiple Matching Method for Observed Glacier Motion with Repeat Image Feature Tracking, *IEEE Trans. Geosci. Remote Sens.*, 55, 2431–2441, 2017.
- Jeong, S. and Howat, I. M.: Performance of Landsat 8 Operational Land Imager for mapping ice sheet velocity, *Remote Sens. Environ.*, 170, 90–101, doi:10.1016/j.rse.2015.08.023, 2015.
- Jones, S. D., Le Quéré, C., Rödenbeck, C., Manning, A. C. and Olsen, A.: A statistical gap-filling method to interpolate global monthly surface ocean carbon dioxide data, *J. Adv. Model. Earth Syst.*, 7, 1554–1575, doi:10.1002/2014MS000416, 2015.
- Joughin, I., Abdalati, W., and Fahnestock, M.: Large fluctuations in speed on Greenland’s Jakobshavn Isbræ glacier, *Nature*, 432, 608–610, doi:10.1038/nature03130, 2004.
- Joughin, I., Das, S. B., King, M. A., Smith, B. E., Howat, I. M., and Moon, T.: Seasonal Speedup Along the Western Flank of the Greenland Ice Sheet, *Science*, 320, 781–784, doi.org/10.1126/science.1153288, 2008.
- Joughin, I., Smith, B. E., Howat, I. M., Floricioiu, D., Alley, R. B., Truffer, M., and Fahnestock, M.: Seasonal to decadal scale variations in the surface velocity of Jakobshavn Isbræ, Greenland: Observation and model-based analysis, *J. Geophys. Res.-Earth Surf.*, 117, 1–20, doi.org/10.1029/2011JF002110, 2012.
- Joughin, I., B. Smith, B., Howat, I., and Scambos, T.: MEaSUREs Greenland Ice Sheet Velocity Map from InSAR Data, Version 2. Boulder, Colorado USA. NASA National Snow and Ice Data Center Distributed Active Archive Center, 2015, updated 2017.
- Khan, S. A., Sasgen, I., Bevis, M., van Dam, T., Bamber, J. L., Wahr, J., Willis, M., Kjaer, K. H., Wouters, B., Helm, V., Csatho, B., Fleming, K., Björk, A. A., Aschwanden, A., Knudsen, P. and Munneke, P. K.: Geodetic measurements reveal similarities between post-Last Glacial Maximum and present-day mass loss from the Greenland ice sheet, *Sci. Adv.*, 2(9), e1600931–e1600931, doi:10.1126/sciadv.1600931, 2016.
- Kjeldsen, K. K., Korsgaard, N. J., Björk, A. A., Khan, S. A., Box, J. E., Funder, S., Larsen, N. K., Bamber, J. L., Colgan, W., van den Broeke, M. R., Siggaard-Andersen, M.L., Nuth, C., Schomacker, A., Andresen, C. S., Willerslev, E., and Kjær, K. H.: Spatial and temporal distribution of mass loss from the Greenland ice sheet since AD 1900, *Nature*, 528, 396–400, doi:10.1038/nature16183, 2015.

- ▲ Korona, J., Berthier, E., Bernard, M., Rémy, F. and Thouvenot, E.: SPIRIT. SPOT 5 stereoscopic survey of Polar Ice: Reference Images and Topographies during the fourth International Polar Year (2007–2009), *ISPRS J. Photogramm. Remote Sens.*, 64, 204–212, doi.org/10.1016/j.isprsjprs.2008.10.005, 2009.
- 5 Krimmel, R., and Rasmussen, L.: Using sequential photography to estimate ice velocity at the terminus of Columbia Glacier, Alaska. *Ann. Glaciol.*, 117–123, 1985.
- Lemos, A., Shepherd, A., McMillan, M., Hogg, A. E., Hatton, E. and Joughin, I.: Ice velocity of Jakobshavn Isbræ, Petermann Glacier, Nioghalvfjærdsfjorden and Zachariæ Isstrøm, 2015–2017, from Sentinel 1-a/b SAR imagery, *Cryosph. Discuss.*, 2087–2097, doi.org/10.5194/tc-2017-251, 2018.
- 10 McFadden, E. M., Howat, I. M., Joughin, I., Smith, B. E. and Ahn, Y.: Changes in the dynamics of marine terminating outlet glaciers in west Greenland (2000–2009), *J. Geophys. Res. Earth Surf.*, 116, 1–16, doi:10.1029/2010JF001757, 2011.
- 15 Moon, T. and Joughin, I.: Changes in ice front position on Greenland’s outlet glaciers from 1992 to 2007, *J. Geophys. Res. Earth Surf.*, 113, F2, doi:10.1029/2007JF000927, 2008.
- Moon, T., Joughin, I., Smith, B., and Howat, I.: 21st-century evolution of Greenland outlet glacier velocities, *Science*, 336, 576–578, doi.org/10.1126/science.1219985, 2012.
- 20 Moon, T., Joughin, I., Smith, B., van den Broeke, M. R., Berg, W. J., Noël, B., and Usher, M.: Distinct patterns of seasonal Greenland glacier velocity, *Geophys. Res. Lett.*, 41, 7209–7216, doi.org/10.1002/2014GL061836, 2014.
- Moon, T., Joughin, I., and Smith, B.: Seasonal to multiyear variability of glacier surface velocity, terminus position, and sea ice/ice mélange in northern Greenland, *J. Geophys. Res. Earth Surf.*, 120, 818–833, doi.org/10.1002/2015JF003494, 2015.
- 25 Morlighem, M., Williams, C. N., Rignot, E., An, L., Arndt, J. E., Bamber, J. L., Catania, G., Chauché, N., Dowdeswell, J. A., Dorschel, B., Fenty, I., Hogan, K., Howat, I., Hubbard, A., Jakobsson, M., Jordan, T. M., Kjeldsen, K. K., Millan, R., Mayer, L., Mouginot, J., Noël, B. P. Y., O’Cofaigh, C., Palmer, S., Rysgaard, S., Seroussi, H., Siegert, M. J., Slabon, P., Straneo, F., van den Broeke, M. R., Weinrebe, W., Wood, M. and Zinglensen, K. B.: BedMachine v3: Complete Bed ▲
▲ Topography and Ocean Bathymetry Mapping of Greenland From Multibeam Echo Sounding Combined With Mass Conservation, *Geophys. Res. Lett.*, 44, 11,051–11,061, doi:10.1002/2017GL074954, 2017.

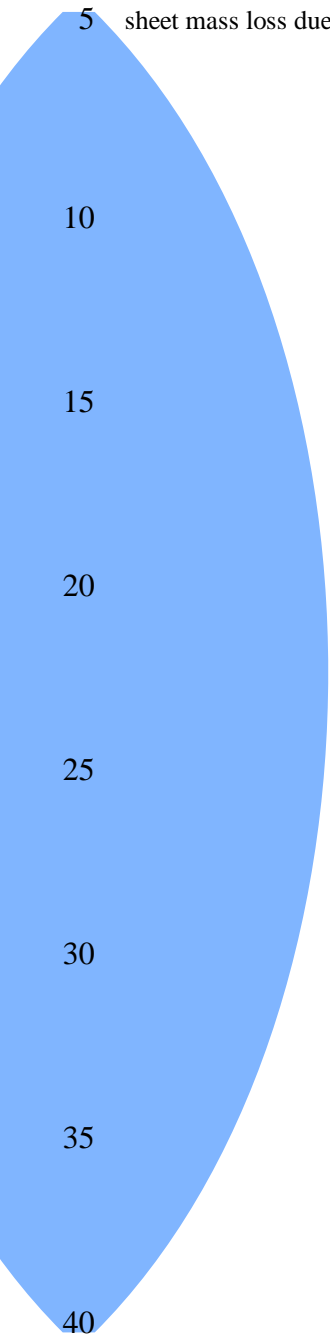
- Mouginot, J., Rignot, E., Scheuchl, B., Fenty, I., Khazendar, A., Morlighem, M., and Paden, J.: Fast retreat of Zachariæ Isstrøm, northeast Greenland, *Science*, 250, 1357-1361, doi.org/10.1126/science.aac7111, 2015.
- 5 Motyka, R. J., Cassotto, R., Truffer, M., Kjeldsen, K. K., Van As, D., Korsgaard, N. J., Fahnestock, M., Howat, I., Langen, P. L., Mortensen, J., Lennert, K. and Rysgaard, S.: Asynchronous behavior of outlet glaciers feeding Godthåbsfjord (Nuup Kangerlua) and the triggering of Narsap Sermia's retreat in SW Greenland, *J. Glaciol.*, 63(238), 288–308, doi:10.1017/jog.2016.138, 2017.
- 10 Münchow, A., Padman, L., and Fricker, H. A.: Interannual changes of the floating ice shelf of Petermann Gletscher, North Greenland, from 2000 to 2012, *J. Glaciol.*, 60, 489–499, doi.org/10.3189/2014JoG13J135, 2014.
- [Nick, F. M., Vieli, A., Howat, I. M. and Joughin, I.: Large-scale changes in Greenland outlet glacier dynamics triggered at the terminus, *Nat. Geosci.*, 2\(2\), 110–114, doi:10.1038/ngeo394, 2009.](#)
- 15 Noh, M. J. and Howat, I.: Automated Coregistration of Repeat Digital Elevation Models for Surface Elevation Change Measurement Using Geometric Constraints, *IEEE Trans. Geosci. Remote Sens.*, 52, 2247–2260, doi:10.1109/TGRS.2013.2258928, 2014.
- 20 Noh, M.J. and Howat, I.: Automated stereo-photogrammetric DEM generation at high latitudes: Surface Extraction with TIN-based Search-space Minimization (SETSM) validation and demonstration over glaciated regions, *GIScience & Remote Sens.*, 52:2, 198-217, doi:10.1080/15481603.2015.1008621, 2015.
- 25 Nguyen, A. T. and Herring, T. A.: Analysis of ICESat data using Kalman filter and kriging to study height changes in East Antarctica, *Geophys. Res. Lett.*, 32, 4–7, doi:10.1029/2005GL024272, 2005.
- Noël, B., van de Berg, W. J., Machguth, H., Lhermitte, S., Howat, I., Fettweis, X., and van den Broeke, M. R.: A daily, 1 km resolution data set of downscaled Greenland ice sheet surface mass balance (1958–2015), *The Cryosphere*, 10, 2361-2377, doi.org/10.5194/tc-10-2361-2016, 2016.
- 30 Noël, B., van de Berg, W. J., van Wessem, J. M., van Meijgaard, E., van As, D., Lenaerts, J. T. M., Lhermitte, S., Kuipers Munneke, P., Smeets, C. J. P. P., van Uft, L. H., van de Wal, R. S. W., and van den Broeke, M. R.: Modelling the climate and surface mass balance of polar ice sheets using RACMO2 – Part 1: Greenland (1958–2016), *The Cryosphere*, 12, 811-831, doi.org/10.5194/tc-12-811-2018, 2018. 

- Palmer, S., Shepherd, A., Nienow, P. and Joughin, I.: Seasonal speedup of the Greenland Ice Sheet linked to routing of surface water, *Earth Planet. Sci. Lett.*, 302, 423–428, doi:10.1016/j.epsl.2010.12.037, 2011.
- Porter, D. F., Tinto, K. J., Boghosian, A., Cochran, J. R., Bell, R. E., Manizade, S. S. and Sonntag, J. G.: Bathymetric control of tidewater glacier mass loss in northwest Greenland, *Earth Planet. Sci. Lett.*, 401, 40–46, doi:10.1016/J.EPSL.2014.05.058, 2014.
- Pritchard, H. D., Arthern, R. J., Vaughan, D. G. and Edwards, L. A.: Extensive dynamic thinning on the margins of the Greenland and Antarctic ice sheets, *Nature*, 461, 971–975, doi.org/10.1038/nature08471, 2009.
- Rignot, E. and Kanagaratnam, P.: Changes in the Velocity Structure of the Greenland Ice Sheet, *Science*, 311, 986–990, doi.org/10.1126/science.1121381, 2006.
- Rignot, E., Box, J. E., Burgess, E., and Hanna, E.: Mass balance of the Greenland ice sheet from 1958 to 2007, *Geophys. Res. Lett.*, 35, L20502, doi:10.1029/2008GL035417, 2008.
- Rignot, E., Velicogna, I., van den Broeke, M. R., Monaghan, A., and Lenaerts, J. T. M.: Acceleration of the contribution of the Greenland and Antarctic ice sheets to sea level rise, *Geophys. Res. Lett.*, 38, L05503, doi:10.1029/2011GL046583, 2011.
- Rosenau, R., Scheinert, M. and Dietrich, R.: A processing system to monitor Greenland outlet glacier velocity variations at decadal and seasonal time scales utilizing the Landsat imagery, *Remote Sens. Environ.*, 169, 1–19, doi:10.1016/j.rse.2015.07.012, 2015.
- Sasgen, I., van den Broeke, M. R., Bamber, J. L., Rignot, E., Sørensen, L. S., Wouters, B., Martinec, Z., Velicogna, I., and Simonsen, S. B.: Timing and origin of recent regional ice-mass loss in Greenland, *Earth Planet. Sc. Lett.*, 333–334, 293–303, 2012.
- Schoof, C.: Ice-sheet acceleration driven by melt supply variability, *Nature*, 468(7325), 803–806, doi:10.1038/nature09618, 2010.
- Stearns, L. A. and van der Veen, C. J.: Friction at the bed does not control fast glacier flow, *Science*, doi:10.1126/science.aat2217, 2018.

- Straneo, F. and Heimbach, P.: North Atlantic warming and the retreat of Greenland's outlet glaciers., *Nature*, 504, 36–43, doi:10.1038/nature12854, 2013.
- 5 Sundal, A. V., Shepherd, A., Nienow, P., Hanna, E., Palmer, S. and Huybrechts, P.: Melt-induced speed-up of Greenland ice sheet offset by efficient subglacial drainage, *Nature*, 469(7331), 521–524, doi:10.1038/nature09740, 2011.
- Sundal, A. V., Shepherd, A., Van Den Broeke, M., Van Angelen, J., Gourmelen, N. and Park, J.: Controls on short-term variations in Greenland glacier dynamics, *J. Glaciol.*, 59(217), 883–892, doi:10.3189/2013JoG13J019, 2013.
- 10 Tedstone, A. J., Nienow, P. W., Gourmelen, N., Dehecq, A., Goldberg, D. and Hanna, E.: Decadal slowdown of a land-terminating sector of the Greenland Ice Sheet despite warming, *Nature*, 526(7575), 692–695, doi:10.1038/nature15722, 2015.
- Thomas, R. H.: Force-perturbation analysis of recent thinning and acceleration of Jakobshavn Isbræ, Greenland, *J. Glaciol.*, 15 50, 57– 66, 2004.
- van Angelen, J. H., van den Broeke, M. R., Wouters, B. and Lenaerts, J. T. M.: Contemporary (1960–2012) Evolution of the Climate and Surface Mass Balance of the Greenland Ice Sheet, *Surv. Geophys.*, 35(5), 1155–1174, doi:10.1007/s10712-013-9261-z, 2014. ↴
- 20 ↴ van den Broeke, M. R., Enderlin, E., Howat, I., Kuipers Munneke, P., Noël, B., van de Berg, W. J., van Meijgaard, E. and Wouters, B.: On the recent contribution of the Greenland ice sheet to sea level change, *The Cryosphere*, 10, 1933–1946, doi:10.5194/tc-10-1933-2016, 2016.
- 25 Walsh, K. M., Howat, I. M., Ahn, Y. and Enderlin, E. M.: Changes in the marine-terminating glaciers of central east Greenland, 2000–2010, *The Cryosphere*, doi:10.5194/tc-6-211-2012, 2012.
- 30 Vaughan, D. G., Comiso, J. C., Allison, I., Carrasco, J., Kaser, G., Kwok, R., Mote, P., Murray, T., Paul, F., Ren, J., Rignot, E., Solomina, O., Steffen, K., and Zhang, T.: Observations: Cryosphere, in: *Climate Change 2013: The Physical Science Basis. Contribution of Working Group I to the Fifth Assessment Report of the Intergovernmental Panel on Climate Change*, edited by: Stocker, T. F., Qin, D., Plattner, G. K., Tignor, M., Allen, S. K., Boschung, J., Nauels, A., Xia, Y., Bex, V., and Midgley, P. M., 4, 317–382, Cambridge University Press, 2013.

Vieli, A. and Nick, F. M.: Understanding and Modelling Rapid Dynamic Changes of Tidewater Outlet Glaciers: Issues and Implications, *Surv. Geophys.*, 32(4–5), 437–458, doi:10.1007/s10712-011-9132-4, 2011.

Wouters, B., Bamber, J. L., van den Broeke, M. R., Lenaerts, J. T. M., and Sasgen, I.: Limits in detecting acceleration of ice sheet mass loss due to climate variability, *Nat. Geosci.*, 6, 613–616, 2013.



5 **Table 1: GrIS-wide and basin-scale (delineated in Fig. S6) cumulative mass changes in Gigatons over the 2003–2016 period, listed as the RACMO2.3p2 SMB component, SMB– D mass balance, and GRACE mass balance estimates. Cumulative mass changes here represent the difference between mean annual 2016 and mean annual 2003 estimates, with a negative value indicating net mass loss. The GrIS* domain includes SMB fields from tundra and detached ice caps.**

	SMB	SMB- D	GRACE
Basin 1	-45 ± 31	-334 ± 32	-202 ± 5
Basin 2	155 ± 42	-266 ± 43	-159 ± 10
Basin 3	744 ± 42	-400 ± 43	-447 ± 38
Basin 4	1645 ± 46	-476 ± 48	-922 ± 34
Basin 5	502 ± 69	-869 ± 71	-841 ± 80
Basin 6	558 ± 27	-823 ± 28	-910 ± 44
GrIS*	3458 ± 258	-3263 ± 259	-3479 ± 280

10

Table 2: Summary of D values for the total GrIS and four distinct regions (see Fig. 3), including the estimated mean annual D in 2000, the maximum D over the 2000–2016 period, and the cumulative D anomaly (ΔD_{2000}) relative to the 2000 estimate. All values are described in units of Gta^{-1} . A negative value indicates a reduction in D relative to the 2000 value.

	2000 D	MAXIMUM D	ΔD_{2000}
southwest	9.5 ± 1	10 ± 1	-7 ± 3
southeast	182 ± 6	238 ± 4	284 ± 17
northeast	53 ± 2	63 ± 2	47 ± 8
northwest	187 ± 5	240 ± 3	343 ± 21
GrIS	440 ± 8	524 ± 9	682 ± 31

15

20

5

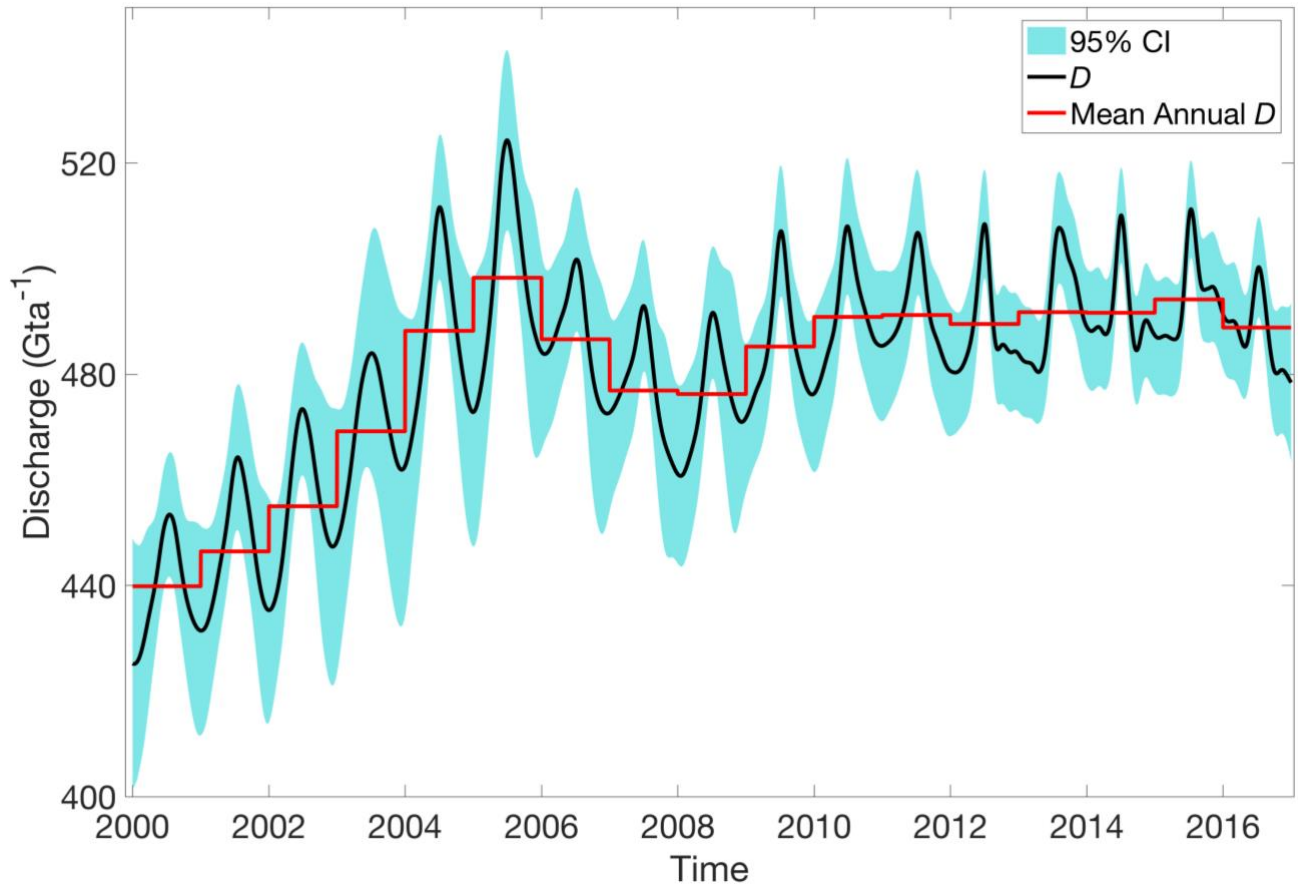
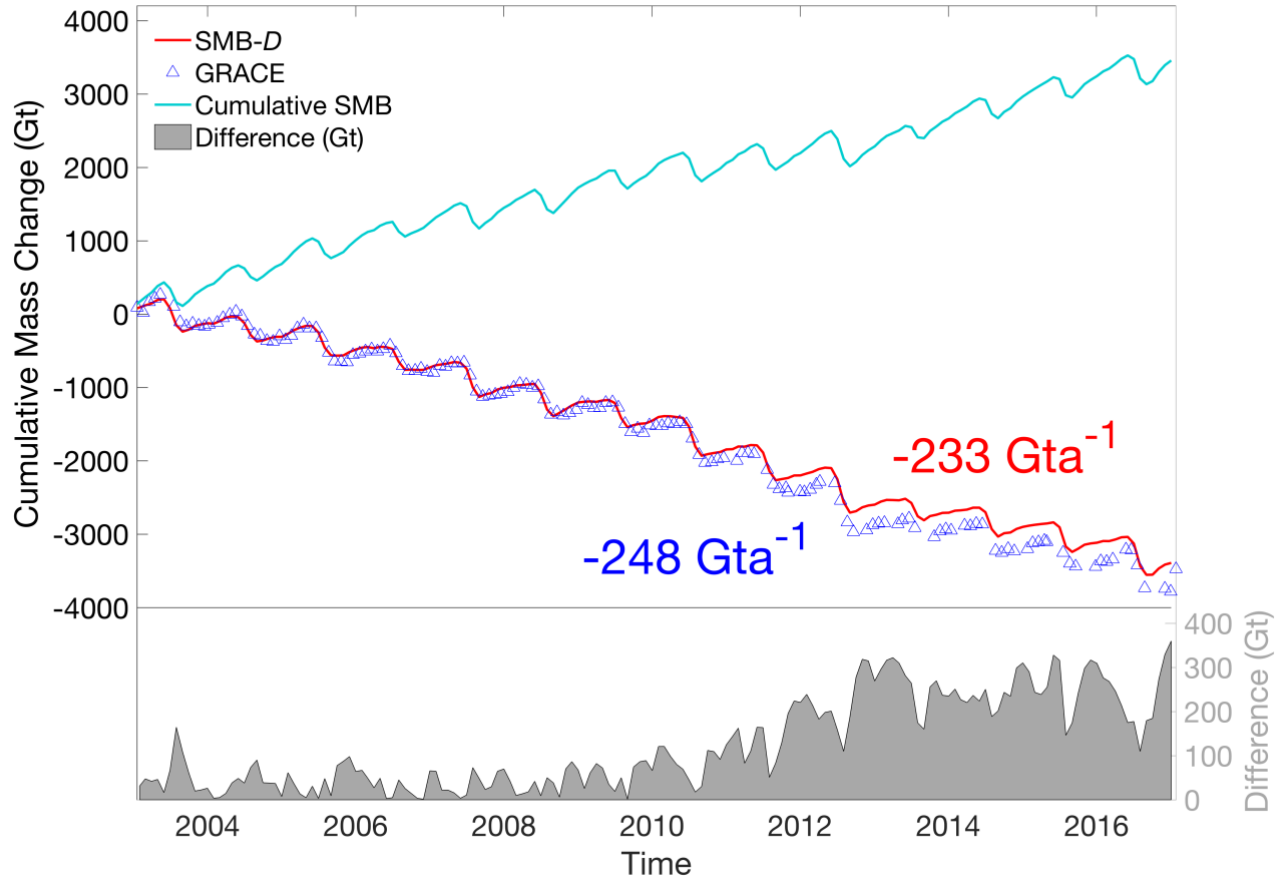


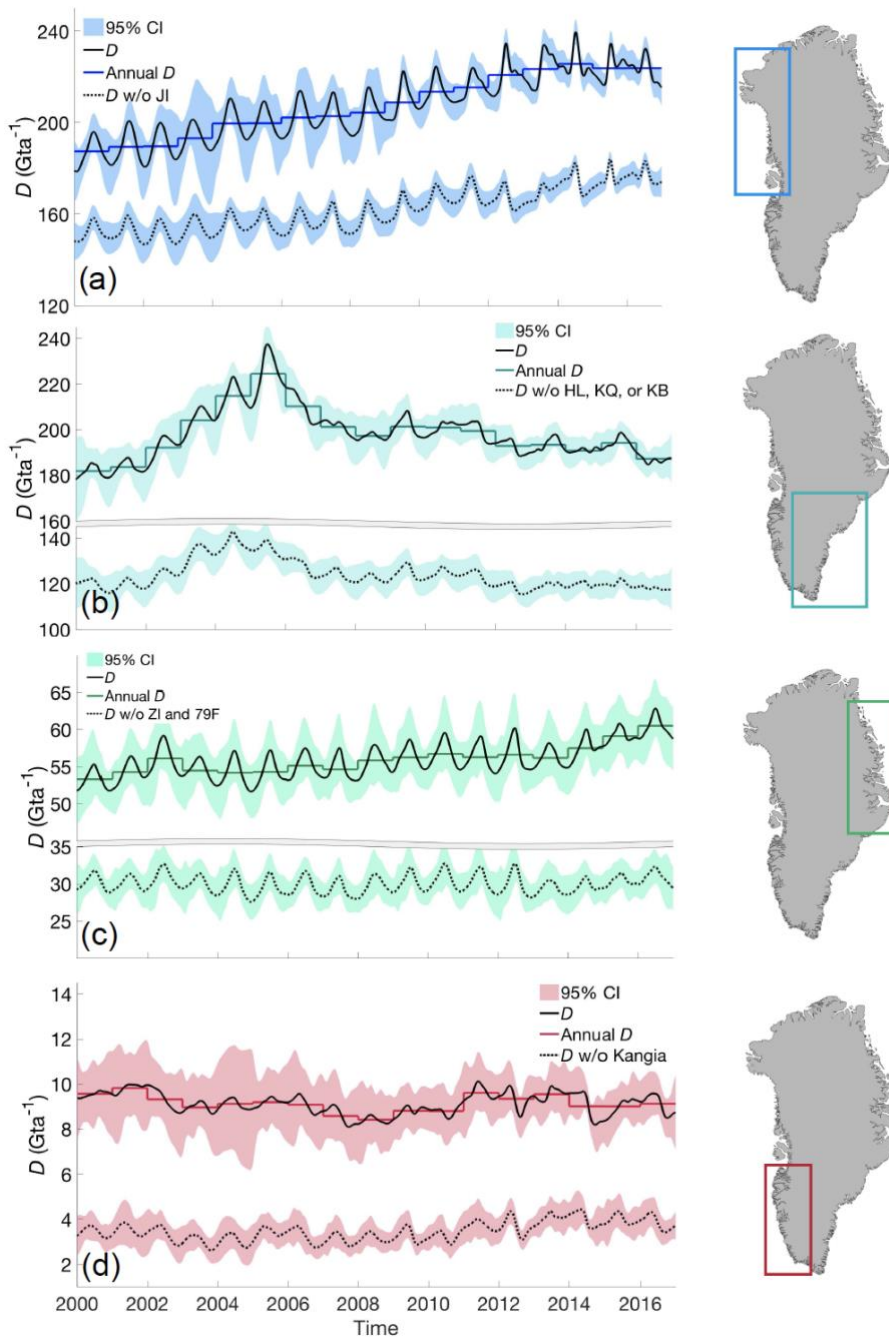
Figure 2: Continuous estimates of discharge, D , for the GrIS for the 2000–2016 period, expressed as a rate of Gigatons per year (Gta⁻¹). Shading represents the 95% confidence interval.

10

15



10 **Figure 2: Comparative cumulative GrIS mass change relative to 2003 between GRACE and monthly SMB-D. Cumulative SMB is also plotted, with cumulative differences between estimates plotted in the lower panel, associated with the right y-axis.**



5 **Figure 3: Net regional D including (solid line) and excluding (dashed line) the dominant glaciers in each region, with shading representing the 95% confidence interval. From top to bottom these regions include: The northwest (a), plotted with and without Jakobshavn (JI), the southeast (b) with and without Helheim (HL), Kangerdlugssuaq (KQ), and the main trunk of Køge Bugt (KB), the northeast (c), with and without Zachariae Isstrøm (ZI) and 79 North (Fjorden) Glacier (79F), and the southwest (d) with and without Kangia Glacier.**

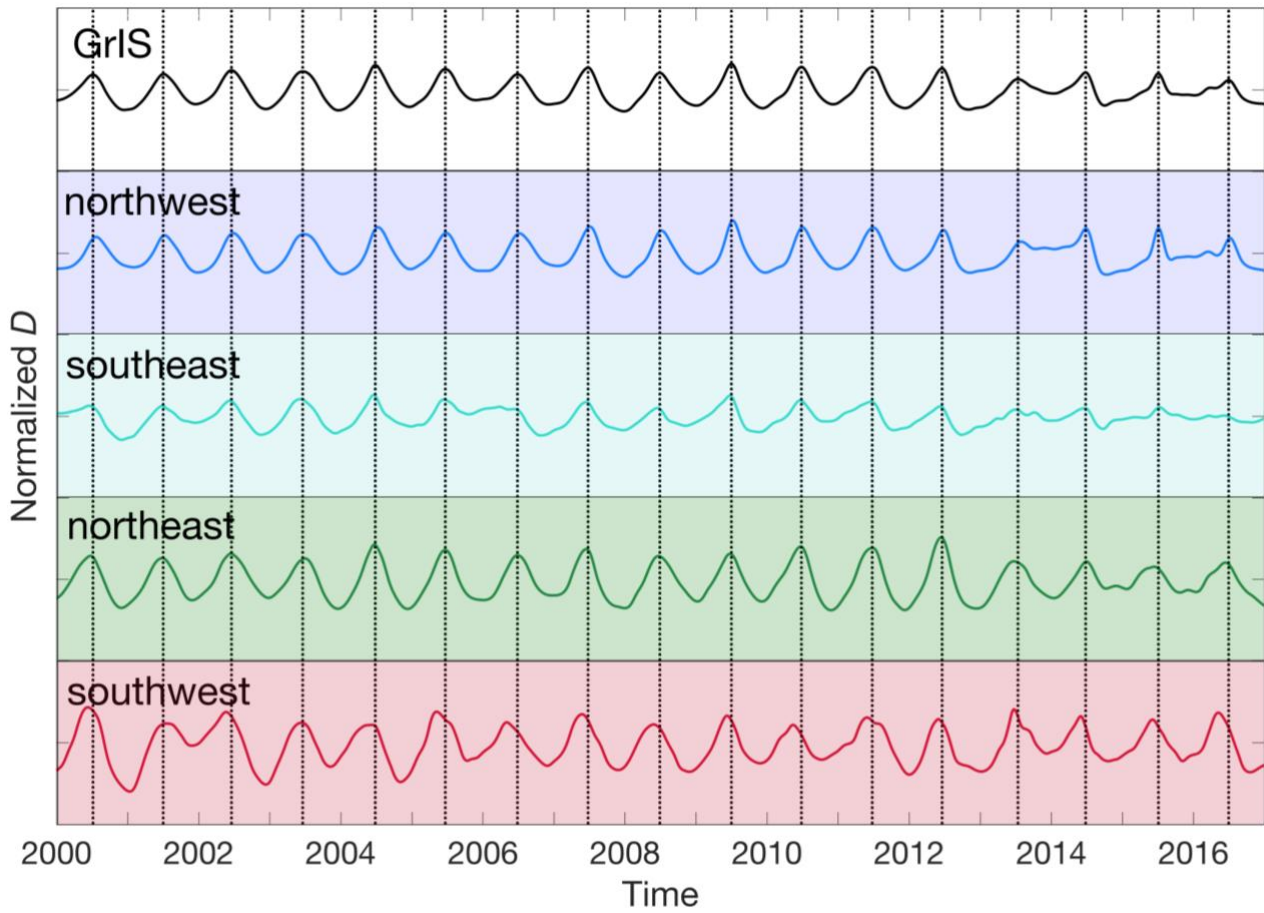
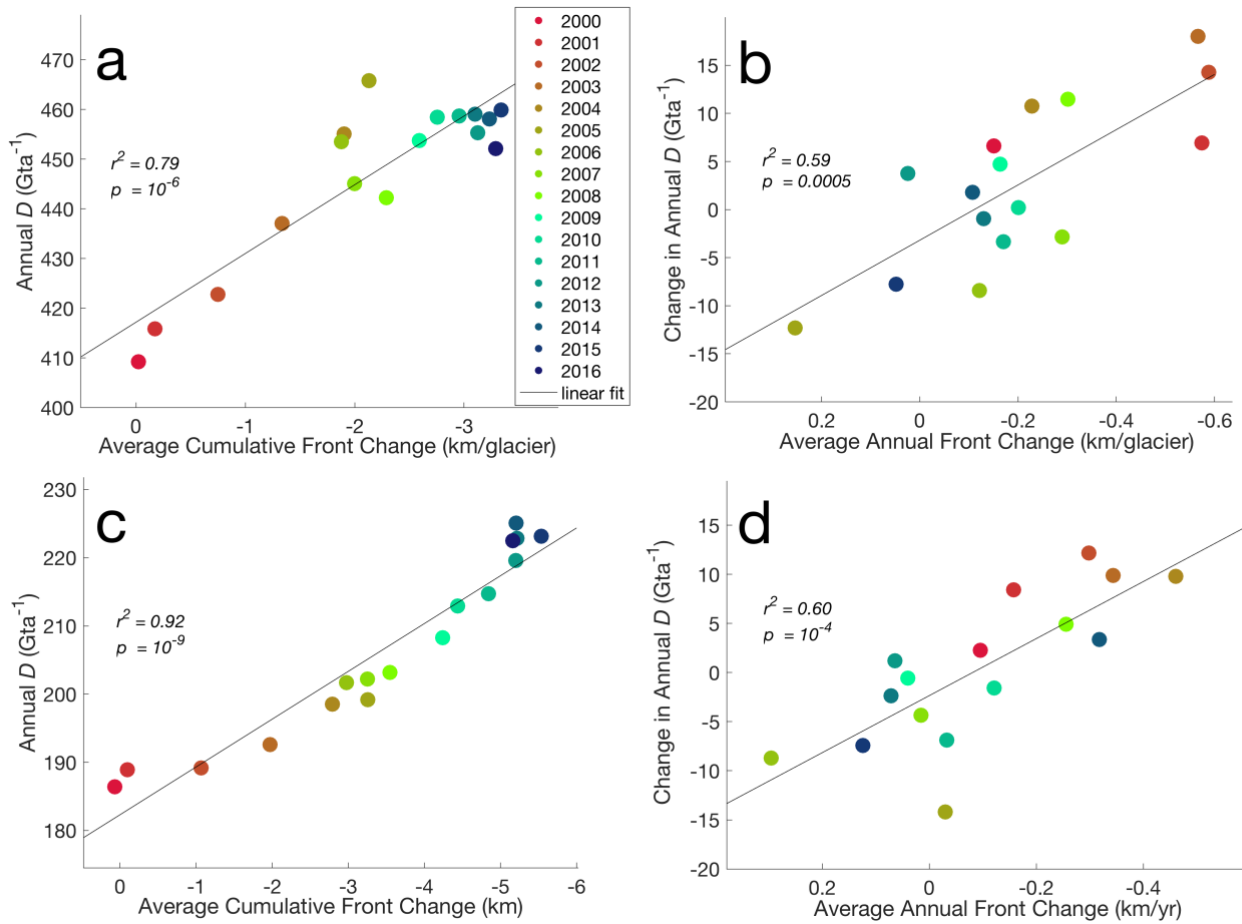


Figure 4: Normalized, detrended D time series for the total GrIS (top), NW (blue), SE (cyan), NE (green) and SW (red) regions. The normalized discharge within each panel spans from -1 to 1 . Vertical black lines align with the annual maximum D of the GrIS-wide series.

5

10



5 **Figure 5: (a) Colored dots are GrIS-wide cumulative average front position change since 1 January 2000, with negative values indicating retreat, versus annual average discharge, D , for each year between 2000 and 2016. The black line is the linear best fit to the data points, with the variance (r^2) and probability value (p) of the fit labelled. (b) The average rate of front position change, with negative values indicating retreat, for each year versus the change in average annual discharge between years. (c) Same relationship described in (a), but for glaciers in the NW region only. (d) Relationship between average front position change and the change in Annual D from the current to the following year ($D_{i+1} - D_i$). Date color scale and statistics for (b), (c), and (d) are as described for (a).**

10

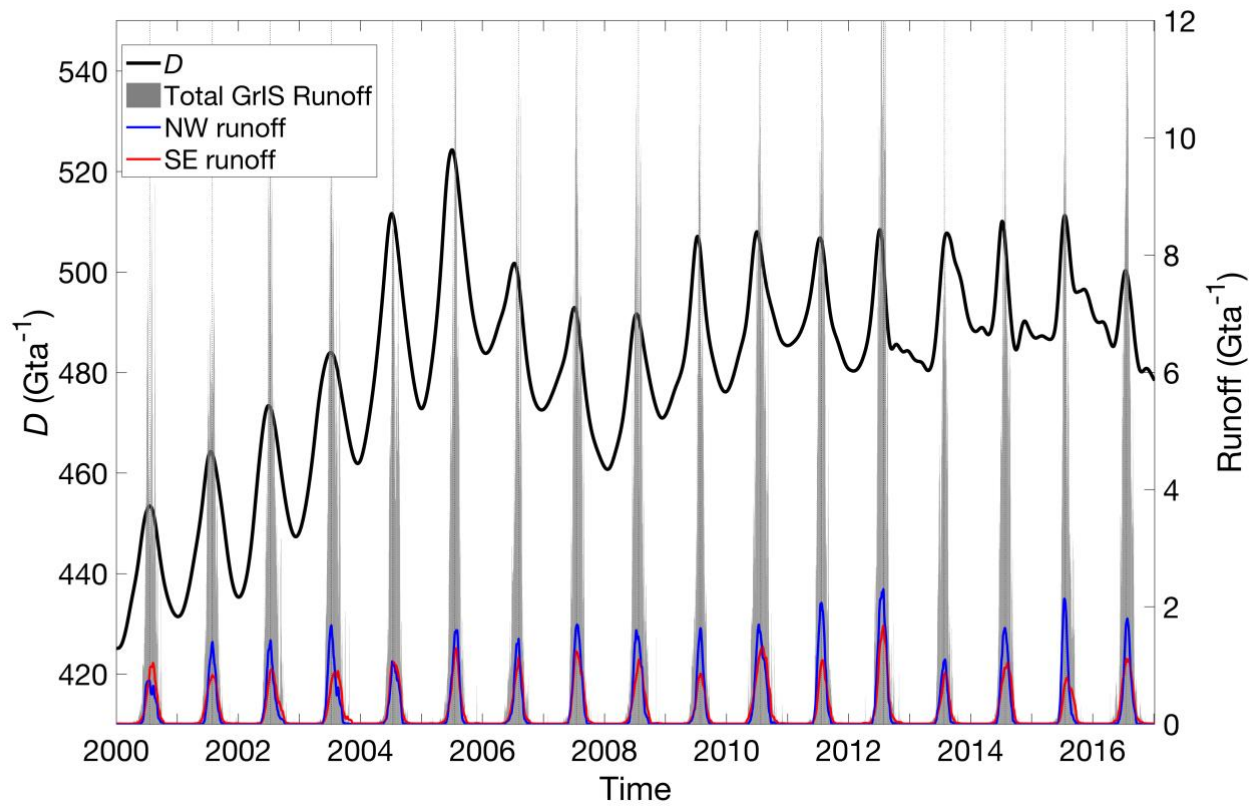


Figure 6: Cumulative GrIS D (black, left y-axis) plotted with raw daily runoff totals (gray bars, right y-axis). The timing of the seasonal maximum runoff is emphasized by vertical dotted lines. Regional runoff totals, smoothed by a 31-day running mean, are shown for the NW and SE region.

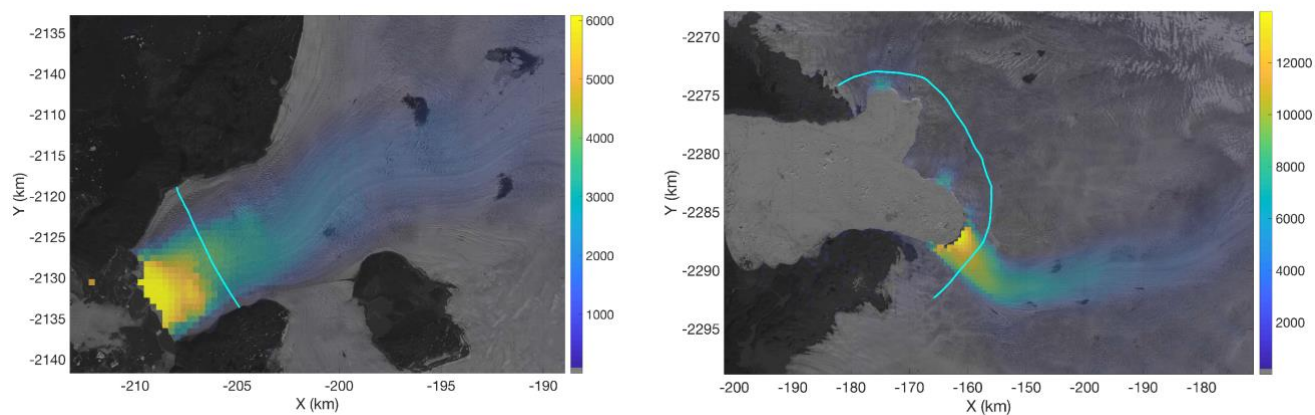
5

10

Supplementary Material

S.1 Glacier Flux Gates

5 A flux gate transect is partitioned into equally-spaced bins approximately 250 m in width. Transects are sampled at a higher spatial resolution for small glaciers (< 4 km wide), and in cases where increased sampling improves the quality of surface elevation data extraction and processing. Ice surface velocity is assumed to be representative of the depth-averaged velocity.



10 **Figure S1: Examples of glacier flux gates (teal) drawn for Store Glacier (left) and Jakobshavn Glacier (right). Underlying scenes depict orthorectified optical imagery of the glacier termini with an overlying velocity map of ice speeds in July 2016, expressed as m a⁻¹.**

S.2 Glacier Velocity

Observations of glacier speed are derived from horizontal velocity maps generated using orthorectified optical imagery from LANDSAT 7, LANDSAT 8, and Advanced Spaceborne Thermal Emission and Reflection radiometer (ASTER) bands 1-3
15 using algorithms described in Jeong et al. (2017). Temporal density is improved by integrating cross-sensor, same-track and cross-path image pairs. Optical observations are augmented by InSAR observations, obtained from the Terra/TandemSAR-X satellite, which become available in 2009. Velocity data, extracted along the multiple coordinate points along the glacier flux gate, are initially filtered by the magnitude of the observational error and the corresponding matching ratio parameter. Errors in the optical observations are a product of the optical imagery quality (noise to pixel ratio), coregistration quality between
20 the paired images, and the velocity of the observed glacier. High signal to noise ratios are common over slow flowing

glaciers. We used a minimum matching ratio threshold of 0.0675 (4 out of 64 successfully matched image pairs), excluding observations with a matching ratio below this threshold from the analysis. Additional observations are removed if their observational errors are excessively large and dominate the variance of the time series. Here, individual observations with errors that exceed three times the standard deviation of the glacier time series are removed. The resulting time series, with outliers removed, may still consist of thousands of observational data points due to the high density of cross-sensor, cross-track optical observations. These series are then smoothed by a running weekly mean filter, weighted by the magnitude of the observational errors.

Despite the high density of optical velocity data, gaps in the time series still exist during winter months when radar-derived glacier speeds are unavailable. A Kalman Filter, a method that has previously been used to estimate height changes in Antarctica from ICESat data (Nguyen et al. 2005), is applied to model reasonable estimates of glacier speed for these missing periods. Modeled ice velocities for missing months are estimated using a linear model of estimated median acceleration for the specific month of interest, derived using a constructed standard seasonality specific to each glacier. To derive the standard seasonality curve, a weighted moving mean filter, weighted by the uncertainties of the respective observations, is first applied to the time series. Next, any existing secular trends in the monthly-resolved time series are removed by subtracting an up to fourth-order polynomial fit from the data, with the polynomial order selected based off a minimum RMSE. Observations in the resulting detrended series are then grouped into bins by month of observation. The standard expected seasonality for each glacier is derived by finding the median value and covariance of each monthly grouping, including months with observations for a minimum of 5 years throughout the time series. Months with fewer available observations will therefore tend to have a higher range of uncertainty. If, throughout the time series, no optical or radar data exist for a particular month, a standard monthly value is estimated by extracting the desired monthly solution from a periodic function fit to the available monthly median values.

The curve is standardized to produce a modelled seasonality of expected incremental change in speed from one particular month to the next. Within the Kalman filter framework, estimates for missing periods are derived by calculating the optimally-interpolated estimate from the two nearest surrounding observations. With the linear model serving as the initial background state, subsequent analyses are performed at each missing monthly time step by using the values and errors of the two nearest available observations to construct the Kalman gain matrix, \mathbf{W} , in Eq. (S1). The Kalman gain is used to appropriately weight the observational innovation, or difference between observations ($y_1^o y_2^o$) and background values at those points ($y_1^b y_2^b$) to produce the analysis at time (t_i) as shown in Eq. (S2). Analysis errors (e_i^a) are similarly derived. The subsequent forecast x_{i+1}^b (and forecast variance σ_{b+1}^2) is computed using the product of the linear model for the month of interest, \mathbf{M} , and the analysis, x_i^a (analysis variance, $\sigma_{a,i}^2$), plus a random model error component, ε_M (model variance σ_{M2}). This forecast becomes the new background state at the next time step, t_{i+1} . The resulting modeled monthly estimates of glacier velocity are appended to the periods of the time series where observational velocity data are available.

$$\mathbf{W}_i = \frac{(\mathbf{B}^o + \mathbf{R})^{-1} \mathbf{b}_i}{\mathbf{b}_i}$$

5 **Equation S1: Kalman Gain, \mathbf{W}** , where denotes \mathbf{B}^o denotes the background error covariance matrix, \mathbf{R} the observational covariance matrix of the two respective observed values used in the analysis, and \mathbf{b}_i as the vector projection of the background error in the observational space onto the model space (midpoint of the missing month requiring analysis).

$$x_i^a = x_i^b + w_{i1}(y_1^o - y_1^b) + w_{i2}(y_2^o - y_2^b)$$

$$e_i^a = e_i^b + w_{i1}(e_1^o - e_1^{bo}) + w_{i2}(e_2^o - e_2^{bo})$$

10 **Equation S2: Calculation of the analysis and analysis error at step i .**

$$x_{i+1}^b = \mathbf{M}(t_i)x_i^a + \varepsilon_M$$

$$\sigma_{b,i+1}^2 = \mathbf{M}^2(t_i)\sigma_{a,i}^2 + \sigma_M^2$$

Equation S3: Forecast and forecast variance, which will serve as the background state in the following analysis ($i + 1$).

15

S.3 Glacier Thickness

Seasonal acceleration of glaciers is often accompanied by dynamical thinning (Pritchard et al. 2009), which can dampen the seasonal increase in D . Although dynamic ice thickness changes are less pronounced than changes in glacier speed, sub-annual changes in ice thickness are resolvable for many of the glaciers sampled. These sub-annual observations of glacier ice thicknesses along the flux gate are also integrated into the discharge time series calculations. We find glacier thickness across the flux gate by differencing surface elevation data with a glacial bed topography product, BedMachine version 3 (Morlighem et al. 2017), which implements a mass conservation approach based on assimilated available ice thickness and seafloor bathymetry data. Surface elevation data along the glacier transects are extracted from ASTER digital elevation models (DEM's), ArcticDEM (www.arcticdem.org) and SPOT-5 DEM's (Korona et al. 2009), where available.

25

Transects of surface elevation are often noisy and prone to erroneous values. Surface elevations at each timestep are first compared to the GIMP DEM (Howat et al. 2014) values, for a first-pass identification of clear outliers. If, at each observational time, there is valid data for at least 25 % of the bins across the flux gate, the data at the time step is passed along for additional filtering and smoothing (Figure S2). Typically, median ice thicknesses across a glacier flux gate follow a semi-smooth curve which increases in thickness toward the centerline. A 3–5 year median surface elevation transect and

30

variance over the 3–5 year window are used to remove noisy, erroneous elevation data by filtering values that fall more than two standard deviations outside the median transect geometry. The temporal range of this window can be increased with consideration to the extent of data sparsity that exists for some glaciers. The bin-dependent z-scores of the remaining, valid data are used to fill missing data along the transect. For example, if the mean z-score of the available surface elevation data at a particular time are found to fall one standard deviation below the 5-year median, values for bins with missing data along the transect would be estimated by subtracting one standard deviation from each specific bin's 3–5 year median elevation. This approach allows for the magnitude of cross-transect variability to be resolved if differential thinning patterns are present, such as more pronounced dynamic thinning near the centerline. The final ice thickness values derived from subtracting bed topography products from the smoothed DEM data, are subject to both random and systematic errors. Here, we estimate a random error of 5 m ($1-\sigma$) for the filtered surface elevation transects. Systematic errors arise from bed topography and vary spatially across the ice sheet, but average 70 m along the sampled flux gates.

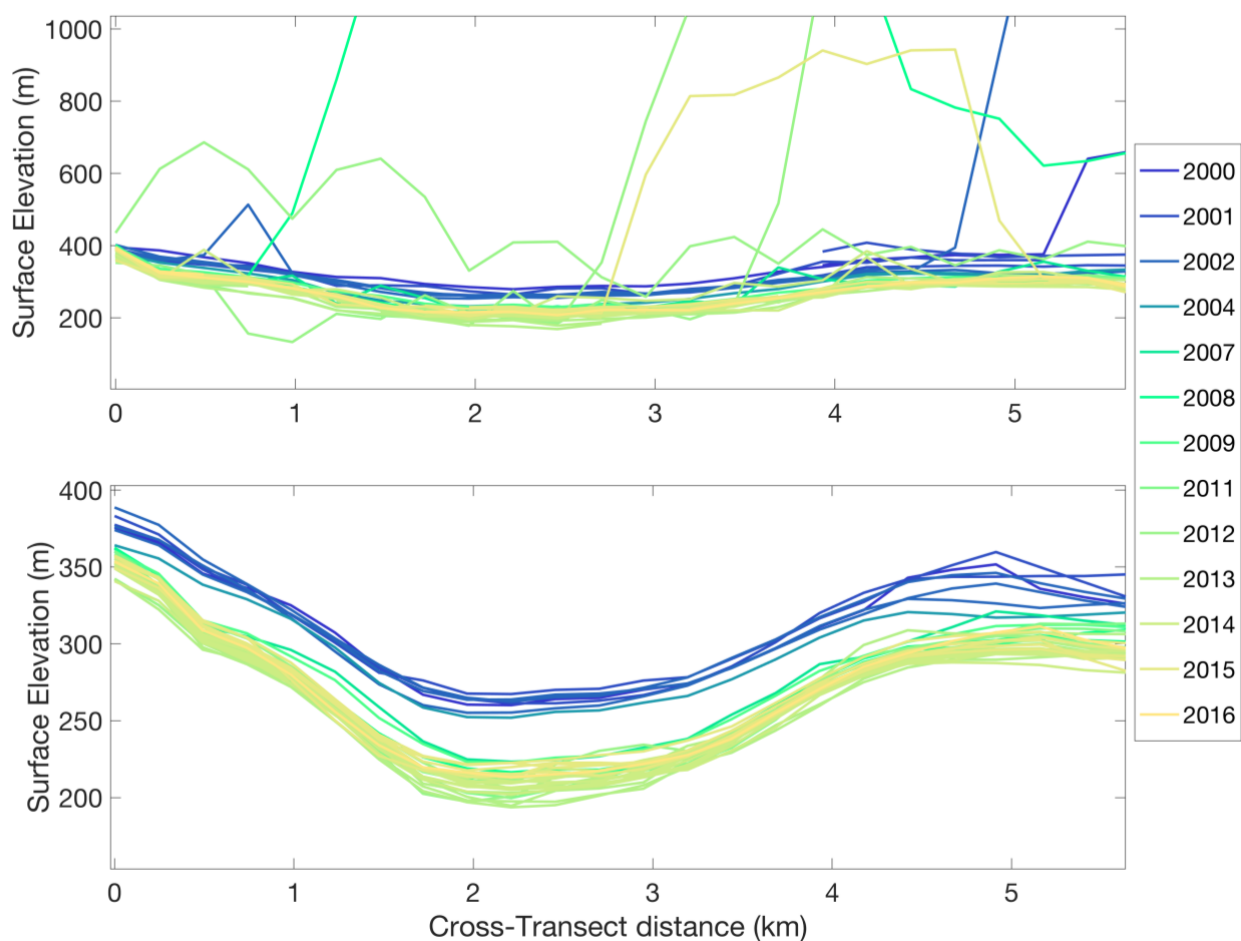


Figure S2: An example of the post-processed surface elevation values (bottom panel) compared to raw data (top panel) across the glacier flux gate transect at Kangia Glacier.

S.4 Derivation of Continuous Discharge Time Series

The continuous glacier velocity time series, now comprised of a combination of modelled and observational data, is of a higher temporal resolution than available ice thickness data. For this reason, observations of ice thickness (h) are linearly interpolated onto the temporal space (t_i) of glacier velocity (v) observations. A record of solid ice discharge at each glacier, Eq. (S4), is then calculated by summing the discharge at each equally-spaced bin (j), with width w , along the glacier flux gate. A constant density (ρ) of 910 kg m^{-3} is assumed with depth.

$$D_{t_i} = \sum_{j=1}^n h_{j,t_i} w_j \vec{v}_{j,t_i} \rho$$

Equation S4

Error in discharge estimates therefore arise from errors in glacier thickness (he) and velocity (ve) retrievals, where ve represents the summed quadrature of the u and v components of displacement. Total discharge error (DE , hereafter to be expressed as 1 standard deviation, σ), is the sum of random (denoted by subscript r) and systematic errors (denoted by subscript s). Random error, Eq. (S5), at each time step is found by summing the errors introduced by both glacier velocities and random errors in ice thickness:

$$DE_{r,t_i} = \sum_{j=1}^n h_{j,t_i} w_j \vec{v}_{j,t_i} \rho + \sqrt{\sum_{j=1}^n (he_{r,j,t_i} w_j \vec{v}_{j,t_i} \rho)^2}$$

Equation S5

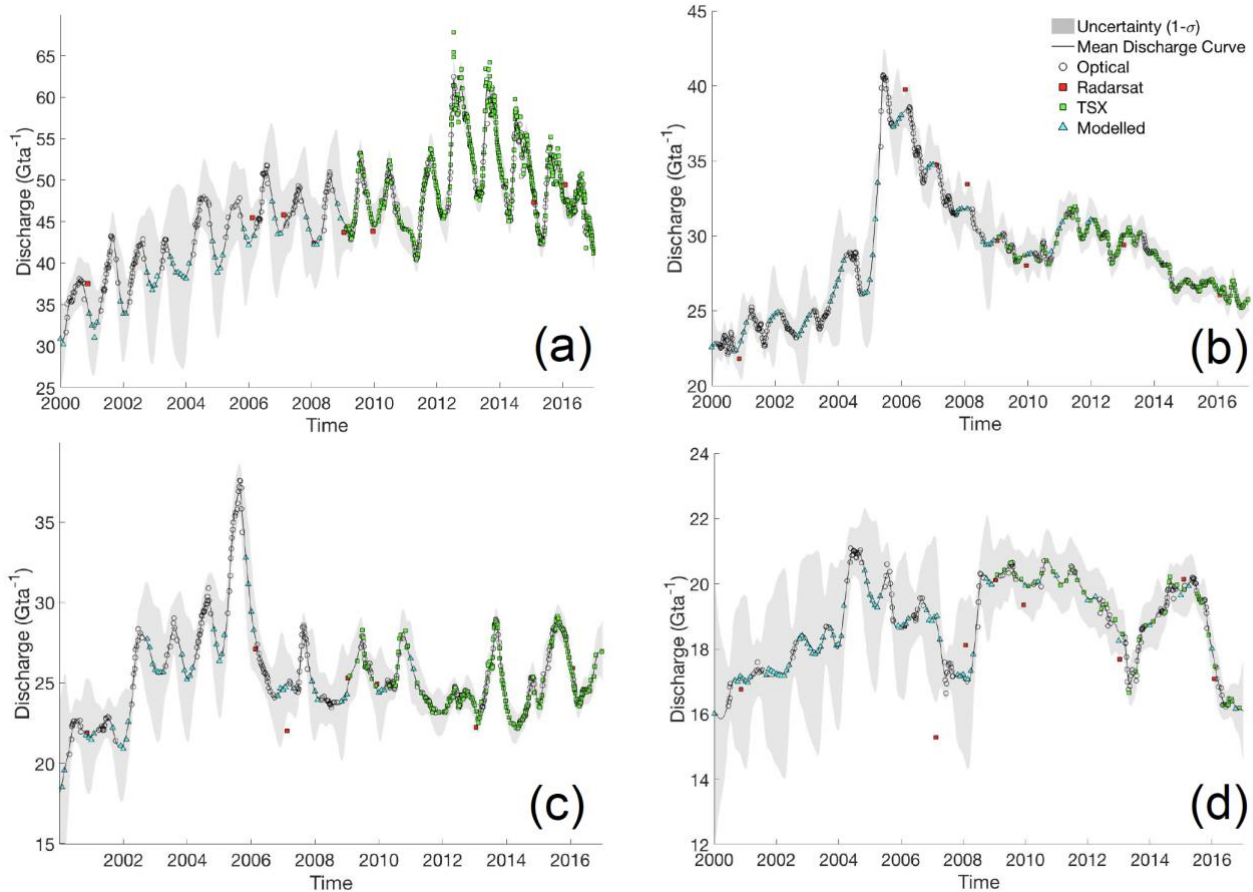
Systematic errors are a result of biases in bed topography retrievals, and are calculated as:

$$DE_{s,t_i} = \sum_{j=1}^n he_{s,j,t_i} w_j \vec{v}_{j,t_i} \rho$$

Equation S6

The discharge time series now include weekly estimates of D for periods when data is available, and monthly modeled estimates for periods of missing data. A Monte Carlo Ensemble is performed for each glacier time series to derive the

continuous discharge curve, which can be sampled at equally-spaced intervals. Using the existing estimates of D and DE , a cubic smoothing spline is fit to the time series. The splines are piecewise cubic functions with continuous first and second derivatives, and are often used to estimate continuous, stochastic processes. For this reason, they are a tool commonly used in climate science (Jones et al. 2015) and can have applications in modelling glaciological process (Krimmel and Rasmussen, 1985; Horgan et al. 2015). A smoothing parameter controls how closely the spline is constrained to observations. The smoothing parameter is determined empirically for each glacier, and typically falls within the range of 0.001–0.005. Smoothing parameter selection is done with consideration given to accommodate the magnitude of individual estimate errors, notable trends, and the time series variance while avoiding overfitting the series. Common problems with spline fits, such as “overshooting” that can arise due to temporal gaps, are largely avoided due to the completeness and semi-uniform spacing of estimates throughout the time series. The described spline fit is repeated for 1000 iterations at each glacier, where during each iteration the function is fit to a new set of perturbed observations, generated by adding normally-distributed random errors sampled from the observational uncertainty, DE . Large individual errors therefore result in a segment of the time series where the spline is less constrained. Lastly, continuous mean estimates of D and the standard deviation, σ , of solutions at each time step are calculated from the 1000-member ensemble (Figure S3). A small subset of glacier time series contains only annually, rather than seasonally, resolved D due to a sparsity of precise velocity observations. This subset includes smaller glaciers mostly along near the central eastern margin and the four northernmost glaciers (Steenby, C.H. Ostenfeld, Academy, and Hagen Brae), and altogether typically contributes $< 10 \text{ Gta}^{-1}$ to the GrIS-wide total.

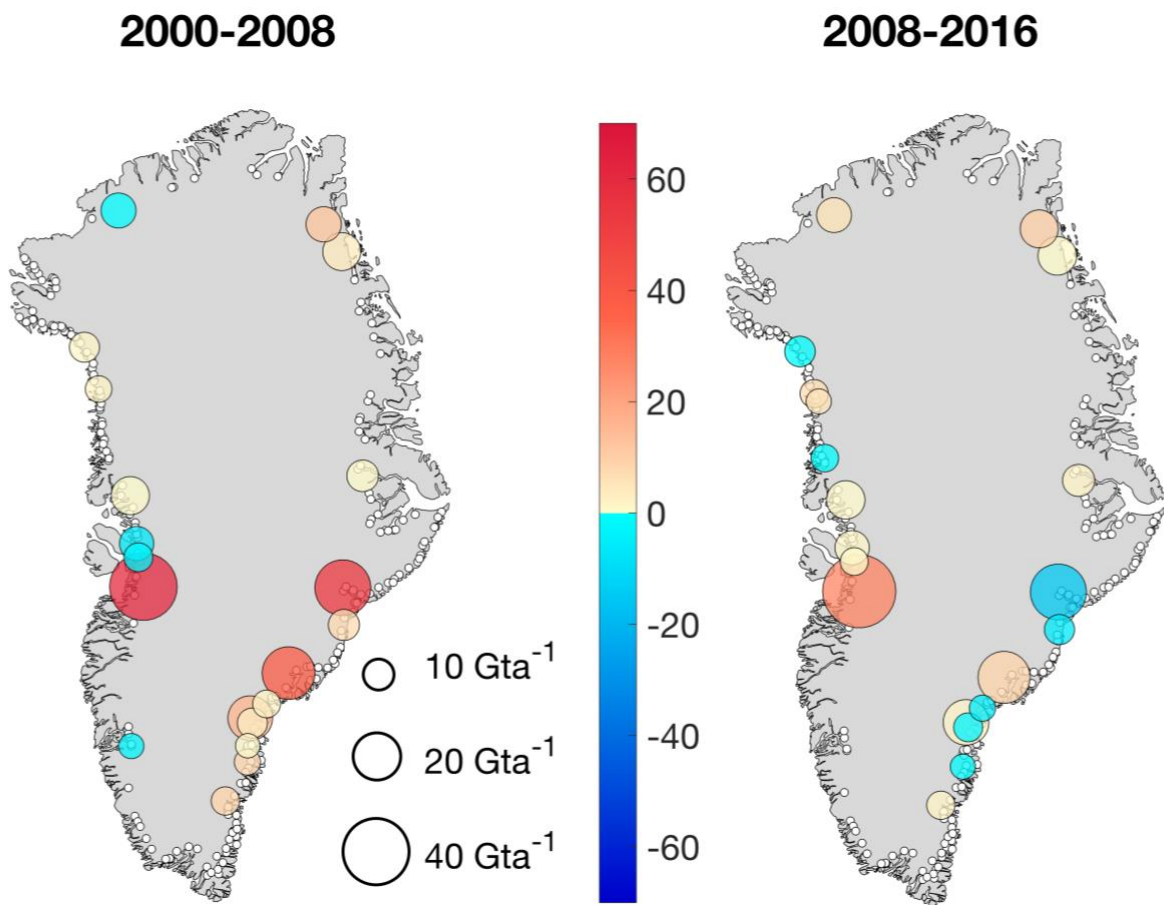


5 **Figure S3: Select solid ice discharge time series for four of GrIS’s largest glaciers: Jakobshavn Isbrae (a), Kangerdlugssuaq (b), Helheim (c), and the central arm of Køge Bugt glacier (d). The series show the resulting continuous time series curve (black), with discharge estimates derived from optical observations, TerraSAR-X, RADARSAT –1 and –2, and modelled estimates. Shading represents uncertainty ($1-\sigma$).**

S.5 Validation

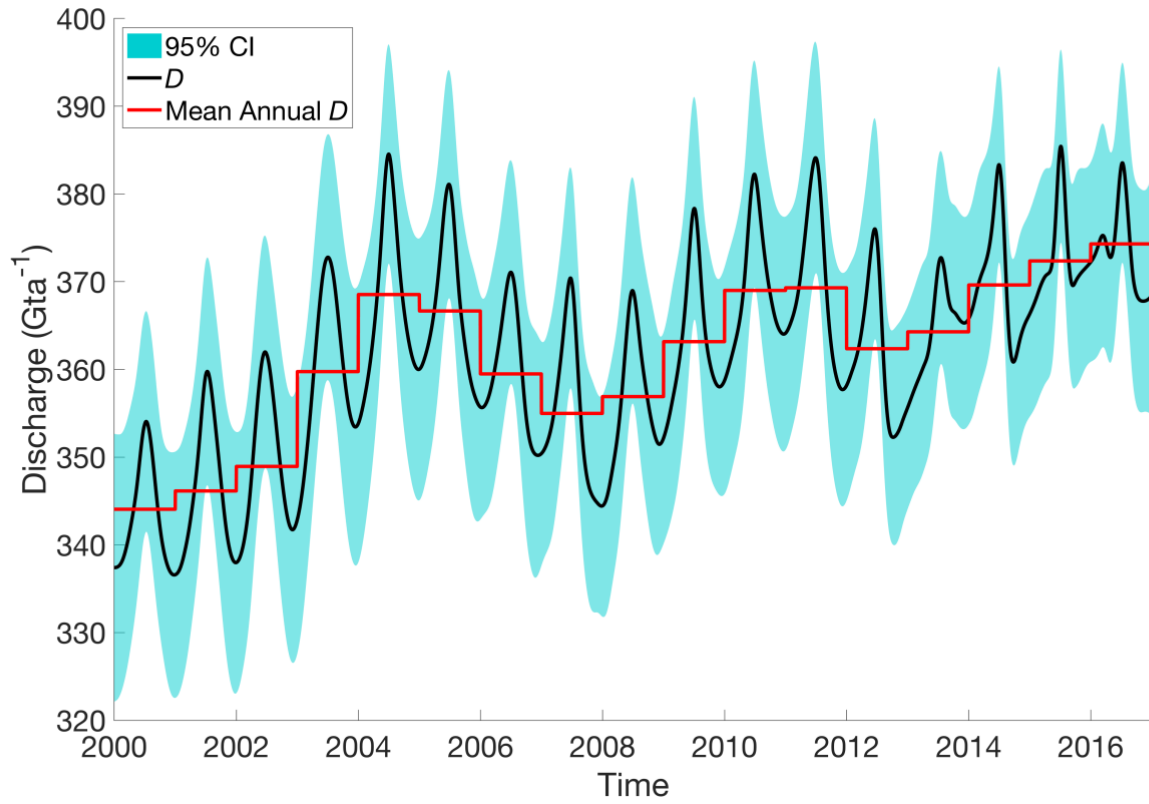
10 Wintertime observations of glacier velocity are available from RADARSAT –1 and –2 (Joughin et al., 2015) for select years of the study. These velocity mosaic products represent the average ice velocity over multi-month periods and are thus not directly appropriate as single point observations for sub-seasonal time series reconstructions. However, these data can serve as an important independent source to validate individual discharge time series. The four mosaics available prior to 2009, and the advent of Terra/TandemSAR-X observations, are particularly useful because they serve as the only existing near ice-sheet wide wintertime velocity observations. Discharge calculated from RADARSAT velocity observations are compared to the derived continuous discharge curves described above by integrating the curves over the individual RADARSAT observational periods. For example, to compare the derived solutions to RADARSAT estimates of D using the

2005/2006 winter velocity mosaic, the total cumulative discharge would be calculated by integrating the values along the curve over the time interval extending from 13 December 2005 through 20 April 2006, corresponding to the observational period of the RADARSAT 2005/2006 campaign. Because RADARSAT observations represent a multi-month average, we assume a constant velocity over the same interval when calculating the radar-derived cumulative discharge. This validation is performed at each glacier for each available RADARSAT mosaic. The wintertime derived discharge estimates are consistent within margins of error with discharge calculated from wintertime RADARSAT observations for 91 % of occurrences. This level of agreement allows for a high degree of confidence in the magnitude of the derived wintertime discharge estimates, which are often the periods that relied most heavily on modeled estimates in lieu of available short-baseline observations.



10 **Figure S4: Spatial distribution of all surveyed glaciers, denoted by a white marker near the flux gate of each glacier. The 20 largest glaciers are shown by colored markers, with the marker size corresponding to the average D over both the 2000–2008 period (left) and 2008–2016 period (right). The color of the markers shows the total D anomaly (in Gta^{-1}) relative to the reference years 2000 (left) and 2008 (right). Positive discharge anomalies indicate increased D relative to the reference years.**

15



5 **Figure S5:** Net dynamic discharge, D_s , for the GrIS excluding the four largest glaciers: Jakobshavn, Kangerdlugssuaq, Helheim, and the central branch of Køge Bugt. The red line displays the annually averaged D_s .

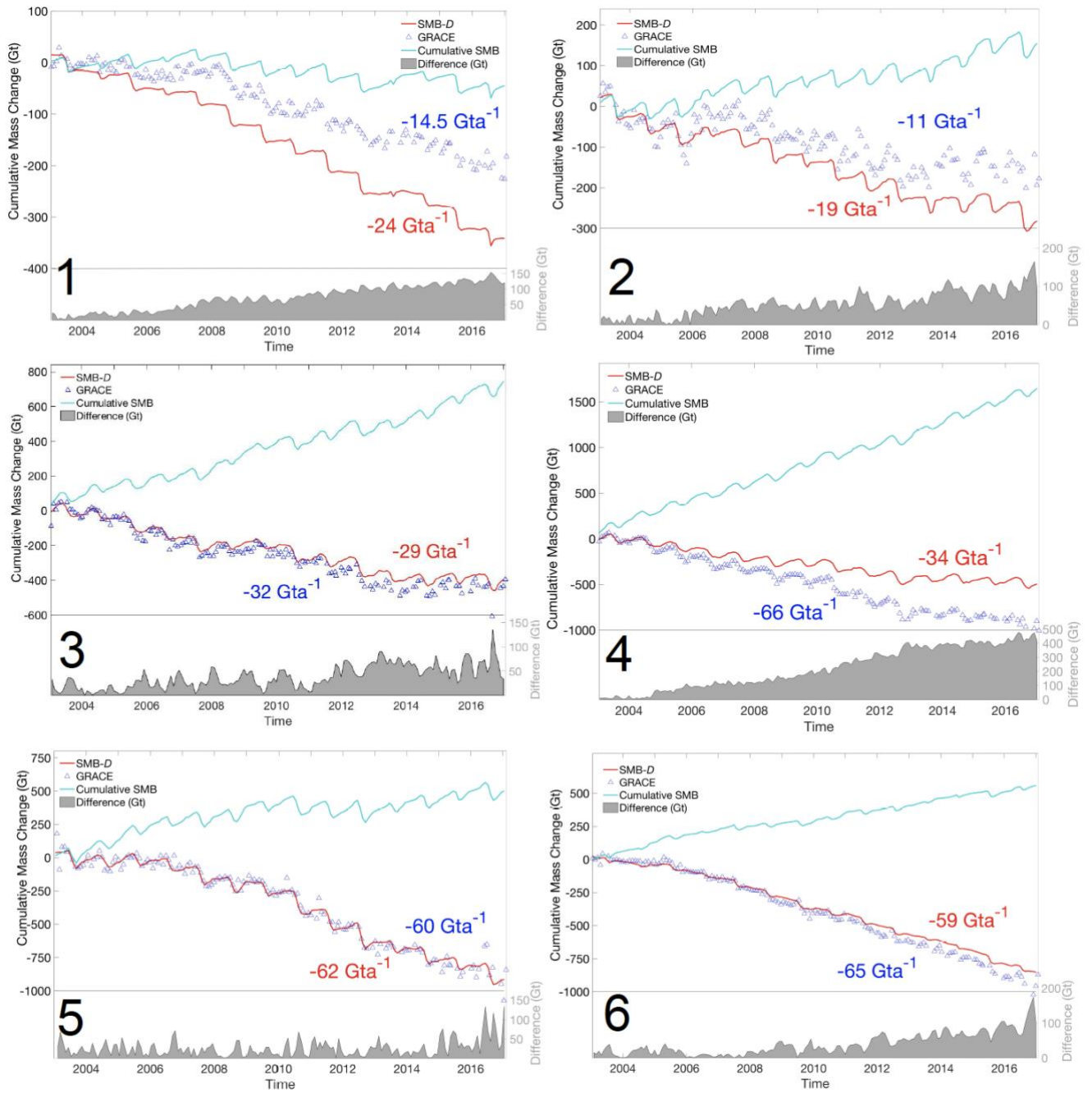


Figure S6: Comparative cumulative mass change relative to 2003 between GRACE, and monthly SMB $-D$ for each of the six GRACE sub-basins, delineated in Figure S6. Cumulative SMB is also plotted, with cumulative differences between estimates plotted in the lower panel, associated with the right y-axis.

5

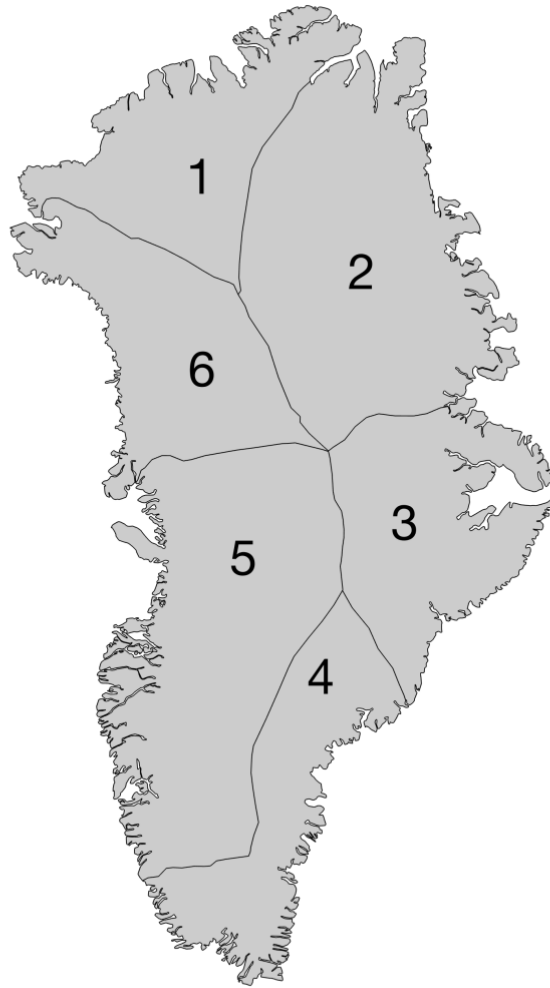


Figure S7: Regional boundaries used in basin-scale SMB $-D$ to GRACE comparisons.

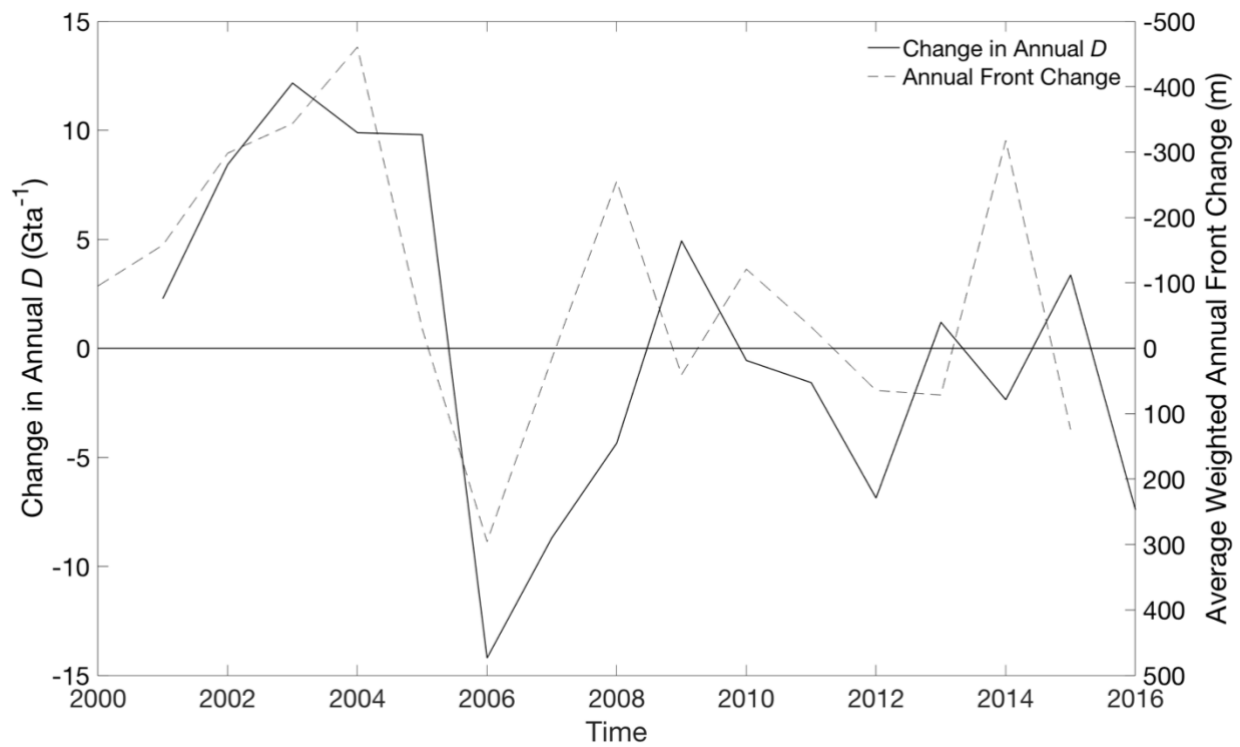


Figure S8: Change in annual D (defined as the difference between the current and previous year's D) in the SE region, and the annual weighted regional front change in meters (right axis). The axis associated with front change is reversed, with negative front change values indicating retreat.

5

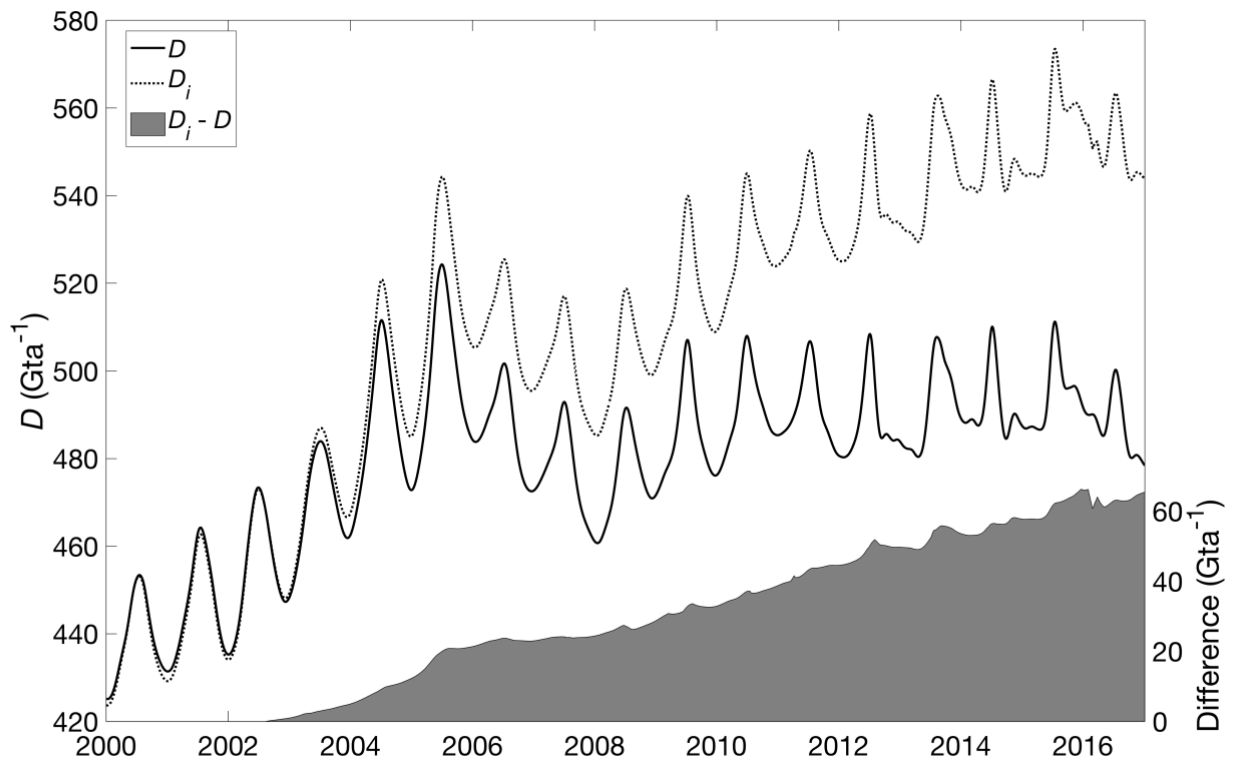
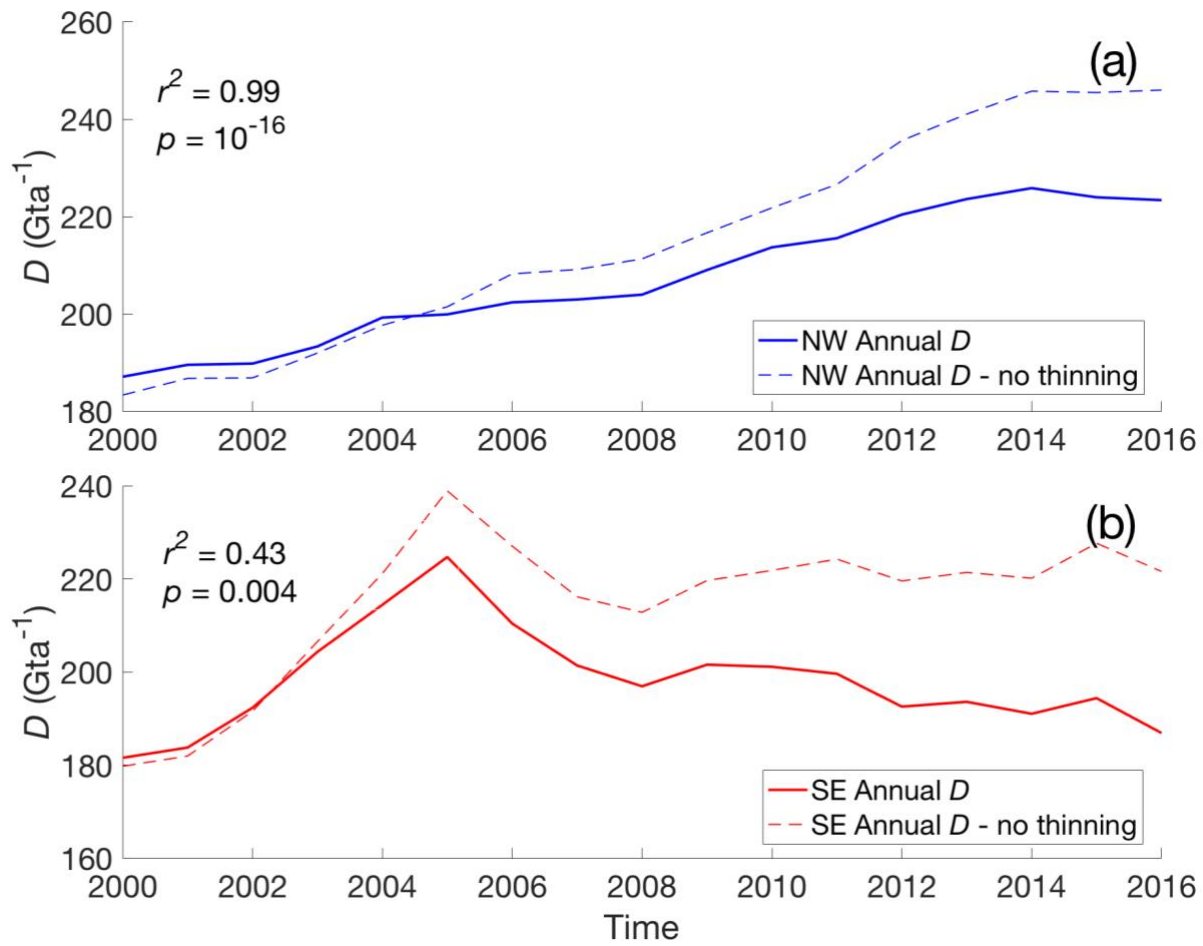


Figure S9: Net GrIS D (solid black) for the GrIS for the 2000–2016 study period, with discharge scaled to remove the effect of thinning, D_i , plotted by the dotted line. Differences between the original and scaled estimates ($D_i - D$) through time are shaded in gray (right axis).



5 **Figure S10:** Annual D and Annual D_i (scaled to remove the effect of thinning) in the NW region (a), and in the SE region (b). Text describes linear correlation and correlation significance between the raw and scaled time series.